



AFRL-OSR-VA-TR-2013-0023

**LARGE TUNABLE DELAYS IN FIBER AND ON-CHIP VIA
CONVERSION/DISPERSION**

**Dr. Alexander Gaerta
Cornell University**

**May 2013
Final Report**

DISTRIBUTION A: Approved for public release.

**AIR FORCE RESEARCH LABORATORY
AF OFFICE OF SCIENTIFIC RESEARCH (AFOSR)
ARLINGTON, VIRGINIA 22203
AIR FORCE MATERIEL COMMAND**

REPORT DOCUMENTATION PAGE

*Form Approved
OMB No. 0704-0188*

The public reporting burden for this collection of information is estimated to average 1 hour per response, including the time for reviewing instructions, searching existing data sources, gathering and maintaining the data needed, and completing and reviewing the collection of information. Send comments regarding this burden estimate or any other aspect of this collection of information, including suggestions for reducing the burden, to Department of Defense, Washington Headquarters Services, Directorate for Information Operations and Reports (0704-0188), 1215 Jefferson Davis Highway, Suite 1204, Arlington, VA 22202-4302. Respondents should be aware that notwithstanding any other provision of law, no person shall be subject to any penalty for failing to comply with a collection of information if it does not display a currently valid OMB control number.

PLEASE DO NOT RETURN YOUR FORM TO THE ABOVE ADDRESS.

1. REPORT DATE (DD-MM-YYYY) 24-10-2008		2. REPORT TYPE Final Performance Report		3. DATES COVERED (From - To) From 24-10-2008 To 12-08-2011	
4. TITLE AND SUBTITLE (DARPA) LARGE TUNABLE DELAYS IN FIBER AND ON-CHIP VIA CONVERSION/DISPERSION				5a. CONTRACT NUMBER	
				5b. GRANT NUMBER FA9550-09-1-0010	
				5c. PROGRAM ELEMENT NUMBER	
6. AUTHOR(S) Dr. Alexander Gaeta				5d. PROJECT NUMBER	
				5e. TASK NUMBER	
				5f. WORK UNIT NUMBER	
7. PERFORMING ORGANIZATION NAME(S) AND ADDRESS(ES) Cornell University - Applied and Engineering Physics Department 270B Clark Hall Ithaca, NY 14853				8. PERFORMING ORGANIZATION REPORT NUMBER	
9. SPONSORING/MONITORING AGENCY NAME(S) AND ADDRESS(ES) AFOSR / RSE 875 North Randolph Street, Suite 325 Room 3112 Arlington, Virginia 22203-1768				10. SPONSOR/MONITOR'S ACRONYM(S) AFOSR / RSE	
				11. SPONSOR/MONITOR'S REPORT NUMBER(S) AFRL-OSR-VA-TR-2013-0023	
12. DISTRIBUTION/AVAILABILITY STATEMENT 1) DISTRIBUTION STATEMENT A: Approved for public release; distribution is unlimited					
13. SUPPLEMENTARY NOTES					
14. ABSTRACT Our recent work on the use of wavelength conversion and dispersive propagation to produce large tunable delays shows great promise for applications that require information to be buffered. In Phase III of the DARPA/DSO slow light program, we propose to extend our work in conversion/dispersion slow light. Our approach will be transparent to OOK and DPSK modulation formats. The frequency conversion will be performed via broadband four-wave mixing (FWM) in Si nanowaveguides. We will develop two different dispersive delay components that are based on optical fiber or on Si waveguides, which will allow us to pursue a communication systems demonstration as well as demonstrating the fundamental ability to achieve significantly longer optical delays than previously achieved in both fiber-based or chipbased systems.					
15. SUBJECT TERMS LARGE TUNABLE DELAYS IN FIBER AND ON-CHIP VIA CONVERSION/DISPERSION; Four-Wave Mixing (FWM); Slow Light Program (DARPA)					
16. SECURITY CLASSIFICATION OF:			17. LIMITATION OF ABSTRACT	18. NUMBER OF PAGES	19a. NAME OF RESPONSIBLE PERSON Tatjana Curcic, RSE (Program Manager)
a. REPORT U	b. ABSTRACT U	c. THIS PAGE U			19b. TELEPHONE NUMBER (Include area code) 703.696.6204

Presented as a Final Performance Report for AFOSR Grant:

FA9550-09-1-0010

**(DARPA) LARGE TUNABLE DELAYS IN FIBER AND ON-CHIP VIA
CONVERSION/DISPERSION**

by

Dr. Alexander Gaeta

Cornell University

Applied and Engineering Physics Department | 270B Clark Hall
Ithaca, NY 14853

to

Dr. Tatjana Curcic

AFOSR / RSE

875 North Randolph Street, Suite 325 | Room 3112
Arlington, Virginia 22203-1768

Submitted 2012.03.21

Spectroscopy of Rb atoms in hollow-core fibers

Aaron D. Slepkov,^{*} Amar R. Bhagwat, Vivek Venkataraman, Pablo Londero, and Alexander L. Gaeta
School of Applied and Engineering Physics, Cornell University, Ithaca, New York 14853, USA

(Received 20 January 2010; published 18 May 2010)

Recent demonstrations of light-matter interactions with atoms and molecules confined to hollow waveguides offer great promise for ultralow-light-level applications. The use of waveguides allows for tight optical confinement over interaction lengths much greater than what could be achieved in bulk geometries. However, the combination of strong atom-photon interactions and nonuniformity of guided light modes gives rise to spectroscopic features that must be understood in order to take full advantage of the properties of such systems. We use light-induced atomic desorption to generate an optically dense Rb vapor at room temperature inside a hollow-core photonic band-gap fiber. Saturable-absorption spectroscopy and passive slow-light experiments reveal large ac Stark shifts, power broadening, and transit-time broadening, that are present in this system even at nanowatt powers.

DOI: [10.1103/PhysRevA.81.053825](https://doi.org/10.1103/PhysRevA.81.053825)

PACS number(s): 32.70.Jz, 42.50.Gy, 42.70.Qs, 42.65.Wi

I. INTRODUCTION

Recently, there have been significant advances in ultralow-light level linear and nonlinear light-matter interactions with hot molecular gases and atomic vapors [1–6]. The main applications driving these efforts include gas sensing [7,8], frequency stabilization [9–11], single- and few-photon nonlinear optical switching [1,2,12,13], and slow light and pulse storage [14,15]. Over the past few years, several approaches have been identified for achieving strong light-matter interactions in confined micro- and nanoscaled geometries. These include photonic interactions with atoms [1,2,16,17] and molecules [3,4,18–21] loaded into hollow-core photonic band-gap fibers and hollow semiconductor waveguides [5,22], and evanescent interactions with species surrounding nanoscale semiconductor waveguides [23], tapered optical fibers (TOF) [6,24], microcavities [25,26], and high- Q optical microresonators [27,28]. The primary motivation of these approaches is to increase the strength of the photonic interactions by maximizing the intensity of the light mode and the interaction length. Hollow waveguide geometries provide for the joint confinement of the light and the atomic or molecular gas of interest in the same physically bounded photonic structure for lengths that can be several orders of magnitude larger than those in conventional bulk focusing geometries [29]. As a result, a significant and growing body of recent work has been dedicated to the study of the spectroscopy [18–21,30,31], nonlinear optical applications [2,4,16,17,32], and gas sensing [8] of atoms and molecules confined to the hollow core of microstructured fibers. Recent reports primarily describe the use of acetylene gas [4,18,20,33] and rubidium vapor [1,2,17,31,34,35], but also include methane [8], hydrogen cyanide [19], ammonia [21], hydrogen [3], and xenon [16]. The utility of hollow semiconductor waveguides, such as that recently demonstrated in hollow $5\ \mu\text{m} \times 12\ \mu\text{m}$ cross-sectional ARROW waveguides [5,22] offers similar advantages, with the added potential for monolithic integration with Si-based photonic circuits. In

the case of evanescent interactions [36], light is most often bound to photonic structures in which the guided mode extends slightly beyond the physical structure, where it can interact with surrounding atoms, molecules, or particles. To achieve this interaction, the photonic structures must be extremely small (on the order of the wavelength of light), and, thus, the evanescent intensities can be sufficiently high as to provide strong nonlinear optical effects [37]. Although in this case, the matter is not confined to the waveguide structure, the interaction region is well defined and confined to within $1\ \mu\text{m}$ of the photonic-device surface. These geometries can, thus, represent an even tighter confinement than in co-confined waveguide geometries.

Clearly, the promise of ultralow-power nonlinear optics makes photon-atom interactions in waveguiding geometries an active and exciting area of research. However, the very nature of these geometries introduces a number of other effects—often undesirable—that pose challenges for applications and interpretations of spectroscopic data: First, the agile loading of atoms and molecules into hollow waveguides often encounters a significant difficulty: Gas kinetics limit the speed with which, for example, hollow-core photonic band-gap fibers (HC-PBGFs) can be pressurized and can be evacuated [38]. Furthermore, significant linewidth broadening of the hot vapors and gases confined to micrometer- and nanometer-length scales is unavoidable. Early studies of acetylene [4] and Rb [17] confined in hollow-core fiber identified collisions with the core walls as the primary broadening mechanism. This effect is inherently connected to transit-time broadening in such systems, and the two are often grouped together. Furthermore, effects such as electromagnetically induced transparency (EIT) [39] that rely on long-lived coherences between closely spaced hyperfine energy levels will experience significant ground-state decoherence if collisions with the walls lead to incoherent population mixing [40]. This broadening is equal to the rate of collisions with the walls, and, thus, scales inversely with the diameter of the waveguide and is directly proportional to the square root of the vapor temperature. As we have previously demonstrated with EIT in warm Rb and acetylene vapor confined to a $6\ \mu\text{m}$ core HC-PBGF, this effect is estimated to be in the range of 15–50 MHz [4,17,34]. Transit-time

^{*}Current address: Steacie Institute for Molecular Sciences, National Research Council of Canada, Ottawa, Ontario, Canada K1A 0R5; e-mail: aaron.slepkov@nrc.ca

broadening occurs when fast-moving particles rapidly traverse the light mode, limiting the photonic interactions to time scales shorter than the natural lifetimes of the system. In the reference frame of the particles, the light appears to be modulated at the transit-time frequency, and, thus, adds new Fourier components that manifest as broadening in the homogeneous linewidth [41]. In the case of hollow-core waveguides, transit-time and wall-collision broadening occur simultaneously, since the light mode only partially fills the core. However, in evanescent interaction geometries—such as for the tapered optical-fiber experiments of Spillane *et al.* [6]—transit-time broadening occurs separately from wall-collision broadening. In this case, where the evanescent light mode is only a few hundred nanometers wide but the vapor is essentially unbounded, transit-time effects dominate and can lead to broadening on the order of 100 MHz. Without cooling or optical trapping, transit-time broadening is unavoidable when light-matter interactions are drastically confined and can become dominant as the light-mode area is minimized [5,6]. Other factors that become relevant at the small volumes and high intensities of systems of this sort include power broadening, mode nonuniformity, and ac Stark shifts. In this paper, we present experimental evidence of the various linewidth broadening mechanisms and shifts that dominate the spectroscopy and the utility of alkali atom vapors confined to the core of an HC-PBGF and discuss their relevance and implications to light-matter interactions in other waveguiding geometries.

II. EXPERIMENTAL

In this paper, we study photonic interactions with room-temperature Rb vapor confined to the $6\ \mu\text{m}$ diameter hollow core of a photonic band-gap fiber, as previously described [17,34]. We mount 45 mm long segments of commercially purchased HC-PBGF designed for guiding light in the range of 750–810 nm (Crystal Fiber, AIR-6-800) inside of an ultrahigh-vacuum steel chamber with glass windows. The chamber pressure is reduced to below 10^{-8} torr, at which point the chamber is exposed to natural Rb metal from a breakseal ampoule, and the system is heated to 45–60 °C, thereby exposing the open fiber ends to a thermal Rb vapor. Figure 1 presents a schematic of our experimental layout. Microscope objectives (New Focus, 16 \times) mounted outside the windows are used to couple light in and out of the fibers, with a total transmission rate of approximately 30%. The output of either fiber face can be imaged onto a CCD to assist with coupling to ensure that the light is coupled into the core mode. A milliwatt-level beam at 805 nm from a tunable cw Ti:sapphire ring laser is coupled into the fiber and is used to generate an on-demand Rb vapor inside the fiber using light-induced atomic desorption (LIAD), as discussed below. The output of a scanning diode laser tuned to span the D_1 line of Rb at 795 nm is split (90:10) and is routed to couple in a counterpropagating direction through the fiber. The stronger (10 nW–1 μW) pump beam combines with the LIAD beam at a polarizing beam cube, and is coupled through the fiber. The weaker (0.2–10 nW) signal beam is coupled through the other end of the fiber, and, using a flip mount, can also be rerouted through the optical cell without passing through the

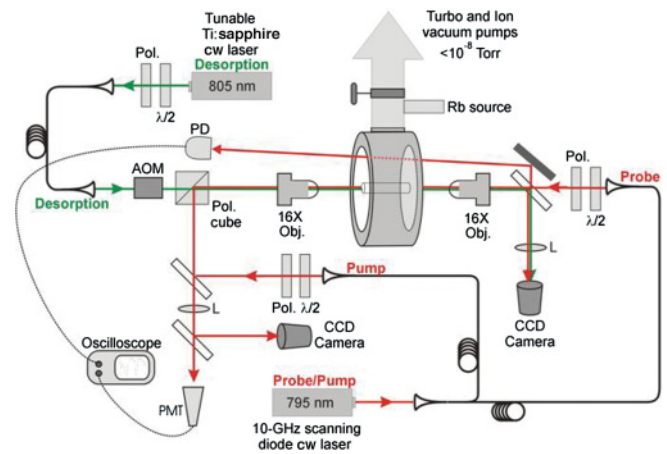


FIG. 1. (Color online) A schematic of the experimental layout: A 4.5 cm long hollow-core photonic band-gap fiber is mounted inside a steel chamber with glass windows connected to an ultrahigh-vacuum system. A 795 nm diode laser beam is scanned mode-hop free over 10 GHz and split into the pump and signal beams, which counterpropagate through the HC-PBGF. An 805 nm light-induced atomic desorption beam is mixed with the pump beam at a polarizing beam cube and is coupled into the fiber with 10 \times microscope objectives. An acousto-optic modulator (AOM) allows for the pulsing of the LIAD beam in order to regulate the optical depth, if needed. The coupling is monitored using a charge-coupled device (CCD) camera. The probe beam can alternately be passed through the cell and can be detected by a photodiode to monitor the ambient cell Rb density. The coupled probe light is detected with photomultiplier tube (PMT), lens (L); photodiode (PD); polarizer (Pol); polarizing beam cube (Pol cube); half-wave plate ($\lambda/2$).

fiber to serve as a monitoring beam for the ambient Rb-vapor density. Once sufficient and repeatable amounts of Rb vapor can be generated in the fiber using LIAD, the cell and the Rb ampoule can be returned to room temperature, and the fiber can be used for weeks without the need for reloading Rb [33].

Rb atoms adsorb onto the inside surface of the fiber but do not establish a stable thermal vapor in the fiber. Instead, a controlled, on-demand, vapor of Rb is generated by applying an off-resonance LIAD beam [42]. Once the fiber is sufficiently loaded with Rb to show a strong desorption with optical depths greater than ~ 100 , the Rb redistributes in the fiber over a period of minutes to hours and can be redesorbed. Once redesorbed, the amount of Rb vapor accessible optically may be depleted, and the Rb is left to redistribute in the fiber. We typically allow a 2 to 3 h redistribution period. Details of this desorption process have been recently described in Ref. [34].

For saturable-absorption spectroscopy, we repeatedly scan the frequency of the diode laser at 100 Hz across the D_1 line and counterpropagate the pump and signal beams. We vary the coupled laser power between 5 and 30 nW for the signal and 10 and 1000 nW for the pump. The probe beam is passed through narrow-band 795 nm filters (TFI 795MC10) and is detected using a PMT. The output of the PMT is coupled to an oscilloscope using suitable impedance termination.

For passive slow-light experiments, we use a slightly modified experimental setup in which a 30 cm long piece of HC-PBGF traverses two UHV optical chambers, as described previously [17]. We carve short, 5 ns, pulses from the same

795 nm diode cw laser using an electro-optic modulator (EOM). This is achieved by driving the EOM (EOSPACE Model PM-OK1-10-PFU-800) with a modulated sinusoidal 10 GHz frequency from an rf generator. The cw signal is modulated by mixing with a 100 ps rise time, 5 ns duration, square pulse, ultimately creating two weak 5 ns pulses at a frequency detuned by 10 GHz on either side of the main laser frequency. Finally, a 400 MHz linewidth, 40 GHz free-spectral-range, solid-state etalon is used as a passband filter for this 5 ns probe pulse, excluding the main laser frequency and opposite sideband pulse. For the pulse-delay experiments, the etalon and the probe pulse frequency are tuned to the center of the D_1 line between the ^{85}Rb $F = 3 \rightarrow F' = 3$ and $F = 2 \rightarrow F' = 2$. The probe pulses are then coupled through the hollow-core fiber and are incident on a PMT for detection. The PMT signal passes through a transimpedance amplifier (FEMTO current amplifier, HCA-200M-20K-C) before being sent to an ultrafast (5 GHz) oscilloscope for data recording.

III. RESULTS AND DISCUSSION

A. ac Stark shifts

The use of LIAD for the generation of a dense Rb vapor inside the fiber allows for the rapid generation of extremely large optical depths in a repeatable manner. In previous work [5,22], groups have relied on a thermal atomic vapor for loading hollow-core semiconductor waveguides or TOFs [6,24], but have obtained small optical depths (ODs) of order of 1 (where OD is defined as minus the natural log of the minimum transmission through the generated vapor). The utility of an alkali vapor for slow-light applications, for example, relies on the ability to generate large optical depths [43]. This suggests that it may prove advantageous to adopt an experimental protocol that utilizes LIAD for vapor generation, and a recent report by Hendrickson *et al.* [24] has already described their need for using LIAD both to obtain Rb vapors and to maintain optical transmission in a TOF experimental system. Thus, the investigation of line-shape broadening and light shifts arising from the use of a relatively strong far detuned desorption beam is relevant for systems beyond HC-PBGF. To obtain the highest optical depth of Rb [33], we use 18–20 mW of coupled 804.5 nm LIAD light. This beam is 10.5 nm detuned from the nearest resonance of Rb (D_1 line at 795.0 nm) and is, thus, described as far detuned. For atomic systems with few-millihertz natural line shapes, 1 GHz is typically considered far detuned. However, 18 mW of light coupled into a hollow waveguide of cross-sectional area on the order of 10^{-7} cm², represents a light intensity of 10^8 mW/cm². By considering that the natural far detuned saturation intensity of the D_1 line of Rb is 4.5 mW/cm² [44], the intensity of our desorption beam can be as much as 8 orders of magnitude larger than this value, and, thus, can yield sizable ac Stark shifts even for 10 nm (4600 GHz) detunings. The ac Stark effect of a given detuned transition, shifts the resonant energy of each coupled level by [45],

$$\Delta v_{\text{ac Stark},i} = \frac{I}{I_{\text{sat},i}} \frac{\gamma_i^2}{8\pi\delta_i}, \quad (1)$$

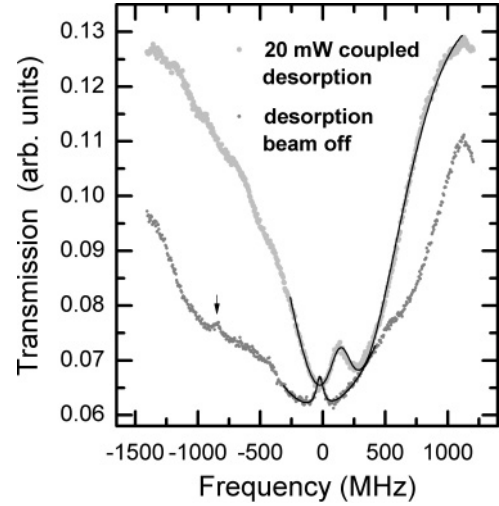


FIG. 2. Saturable-absorption spectroscopy of the ^{87}Rb $F = 1 \rightarrow F' = 2$ transition in the presence and the absence of a 20 mW desorption beam. In the presence of LIAD, a significant ac Stark shift is observed, and the line shape is seen to broaden and to distort. The arrow indicates the ^{87}Rb $F = 1 \rightarrow F' = 1$ transition. Solid lines are fits to a Lorentzian peak inside a Gaussian.

and in total shifting by

$$\Delta v_{\text{ac Stark},i} = \sum_i v_{\text{ac Stark},i}, \quad (2)$$

where I is the light-mode intensity, $I_{\text{sat},i}$ is the saturation intensity of i th transition, γ_i is the natural lifetime of the atoms in level i , and δ_i is the frequency detuning of the strong light beam from the i th transition. To calculate the Stark shift imparted on the D_1 line, we must also consider the coupling to the D_2 transition at 780 and 25 nm away.

As we have previously reported [34], when a strong desorption pulse is used to generate a large Rb density, a residual vapor can remain in the core for a second or more. This allows us to study the line shape of the saturable-absorption peak in the absence of the LIAD beam. Figure 2 shows the effects of the strong desorption beam on the line shape of the saturable-absorption signal both in the presence and in the absence of an ~ 20 mW desorption beam. In the presence of LIAD, the peak is both shifted and considerably broadened, as compared to that without a desorption beam. These data are well described by a simple line-shape approximation of a narrow Lorentzian subtracted inside a wider (Doppler profile) Gaussian, as seen in Fig. 2. In the presence of a 20 mW desorption pulse, the experimental ac Stark shift is approximately 180 MHz, and the line-shape full width at half maximum (FWHM) broadens nonuniformly from 35 ± 2 MHz (in the absence of LIAD) to ~ 150 MHz. By using Eqs. (1) and (2) and considering our use of linearly polarized light, we expect a 90 MHz ac Stark shift in total when summed over all relevant level coupling in the D_1 and D_2 lines. Thus, our experimental shift is considerably larger than would be expected from a simple calculation using average mode powers. We believe that the source of this discrepancy resides in the nonuniformity of the guided HC-PBGF mode. Typical high-resolution saturable-absorption spectroscopy experiments conducted in bulk vapor cells

require the two beams to be near-ideally counterpropagating in order to eliminate residual Doppler signals [46], and the weak signal beam is typically focused smaller within the pump beam to approximate the sampling of a uniform pump mode. Conducting such an experiment in a hollow waveguide offers guarantees that the two beams will always be in a strict counterpropagating geometry. However, this geometry also ensures that the signal and pump modes will be near-perfectly overlapped, and, thus, neither can approximate a uniform (constant power) mode. Instead, the beams propagate as approximate Gaussian-intensity modes [47].

Since the ac Stark shift is proportional to the local intensity, the shift will be strongest for atoms near the center of the light mode and weaker for atoms near the core walls. This readily produces two effects: First, the nonuniformity of the mode leads to a nonconstant Stark shift across the fiber diameter, and, thus, to significant reshaping and inhomogeneous broadening of the saturated absorption peak; second, the peak of the resulting signal is shifted considerably farther than would be expected from Eqs. (1) and (2). Both of these effects are clearly observable in the 20 mW LIAD signals shown in Fig. 2. To model the effect of a realistic core mode on the ac Stark shift of a Lorentzian resonance, we integrate the ac Stark shift as a function of a Gaussian-radial-intensity profile, as weighted by the radial density of Rb atoms ($2\pi r dr$ assuming uniform density). In this case, the experimental core mode is approximated by a Gaussian-intensity profile with a half-width-at-half-maximum radius of $1.0 \mu\text{m}$ that fills the majority of the hollow core without significant extent beyond the physical boundaries of the $3 \mu\text{m}$ radius core walls [47]. As seen in Fig. 3, the simulated shifts given by a uniform average power mode and by a Gaussian-core mode are very different and accurately represent the experimental peak shapes presented in Fig. 2.

We have obtained saturated absorption profiles for a series of LIAD powers ranging between 4 and 19 mW. For each desorption power, the signal is fitted as in Fig. 2, and the total shift is extracted from the peak position of the fit. As shown in

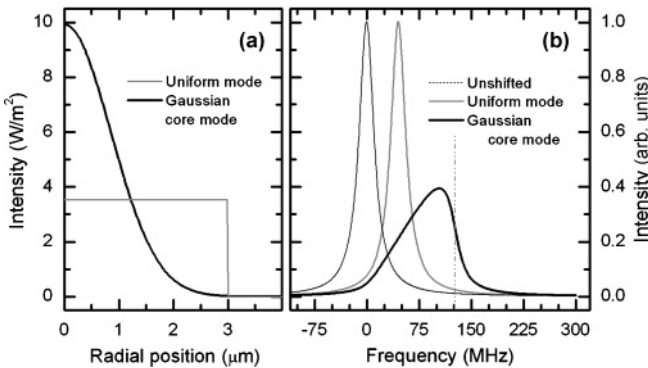


FIG. 3. The effect of guided mode nonuniformity on the ac Stark shift. (a) Radial mode profiles for 10 mW flat-top and Gaussian-core modes. (b) Simulated ac Stark shifts of a Lorentzian saturated-absorption peak by flat-top and Gaussian-core modes. The vertical dashed line represents the maximum shift experienced by the most intense component of the core mode. The nonuniformity of the core mode is also seen to broaden and to steepen the line toward higher frequencies.

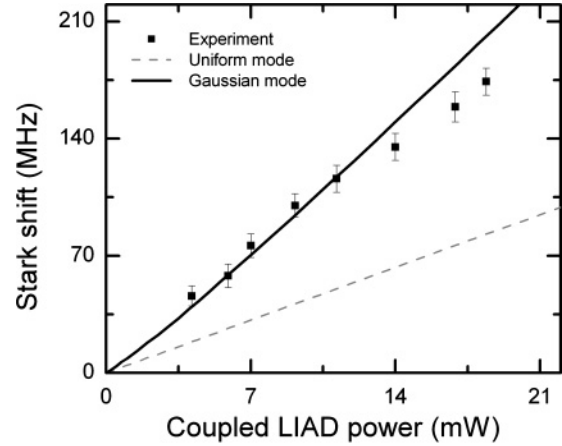


FIG. 4. ac Stark shifts as functions of desorption beam power. 30-nW and 150-nW powers were used for the counterpropagating signal and the pump beams, respectively. The experimental shifts are larger than those expected for a flat-top mode (dashed line) and are well fit by the simulated shift of a nonuniform Gaussian-guided mode (solid line).

Fig. 4, the experimental Stark shift is quasilinear and is well approximated by our nonuniform mode simulation. Overall, we find that with the intense desorption powers necessary for the generation of large Rb optical densities in hollow-core fibers, light shifts on the order of hundreds of megahertz can be induced. This represents both a shift and a broadening that are many times the natural linewidth of the transitions of interest, and the effect must, thus, be considered when using milliwatt-level desorption beams for the generation of large atomic vapor densities.

B. Power broadening and transit-time broadening

One of the main advantages of working with confined waveguiding geometries is the potential to operate in a regime where nonlinearities can be produced at extremely low powers. Power broadening becomes significant when the light intensity exceeds the saturation intensity of the medium, which, for alkali atoms confined within micrometer-sized light modes, can be as low as a few nanowatts. Molecular gases are typically weaker absorbers by several orders of magnitude, and, thus, have much higher saturation powers than alkali atoms. Typical reported saturation powers for acetylene in a $10 \mu\text{m}$ core HC-PBGF are 20–50 mW [19,20]. Significant power broadening has been reported in saturated absorption spectroscopy of molecules loaded into a hollow-core fiber [19–21,24,30]. Figure 5 presents an analysis of linewidth broadening as a function of pump power for saturable-absorption spectroscopy on the ^{87}Rb $F = 1 \rightarrow F' = 2$ transition in our system. To avoid the aforementioned broadening due to the combination of mode nonuniformity and the ac Stark shift, these data were taken with post-LIAD residual vapor, as shown in the bottom curve of Fig. 2. The power-broadening scales as

$$\Delta\nu = \gamma(1 + P/P_{\text{sat}})^{1/2}, \quad (3)$$

where $\Delta\nu$ is the experimental FWHM of the (quasi-) Lorentzian linewidth, γ represents the linewidth in the absence

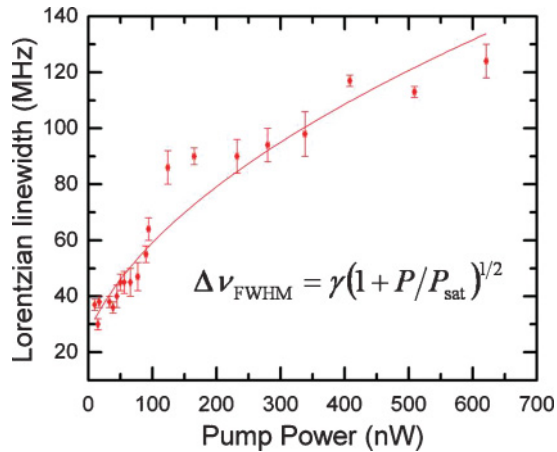


FIG. 5. (Color online) Measured power broadening of Rb atoms confined to the core of the band-gap fiber and predicted linewidth broadening as a function of pump power measured via saturable-absorption spectroscopy on the ^{87}Rb $F = 1 \rightarrow F' = 2$ transition in our system. The intercept represents the minimum linewidth available limited by transit-time broadening.

of power broadening, and P_{sat} is the saturation power of the interaction geometry [48]. Typically, γ is the natural linewidth of the medium (~ 5.75 MHz for the D_1 line of Rb), but, in the more general case, it is the homogeneous linewidth in the absence of light. In our case, this value represents the lower limit on the linewidth resulting from transit-time broadening, and, thus, represents an additional measurement of this effect. By fitting the data in Fig. 5 to the expression in Eq. (3) yields values of 27 ± 3 MHz and 26 ± 7 nW for the transit-time broadening and saturation power, respectively. As discussed earlier, a strict interpretation of the observed saturation power may be misleading, since as with the case of the ac Stark shift, mode nonuniformity will lead to deviations from the simple expression of Eq. (3). Nonetheless, this observed saturation power is an order of magnitude larger than that expected from the natural lifetime of Rb, yet is many orders of magnitude smaller than that observed in bulk vapor cells. It is also 6 orders of magnitude smaller than that observed for molecules in similar core-sized HC-PBGFs, as mentioned previously. This increase in saturation power is derived from the increased homogeneous linewidth from transit-time broadening. A value of 27 ± 3 MHz of transit-time broadening agrees well with our prior estimates obtained from geometric considerations and global fits to absorption spectra [34]. This value represents the narrowest line shape available for Rb atoms in a $6 \mu\text{m}$ confined geometry. As a result, most light-matter interactions in confined micro- and nanoscaled geometries will suffer this transit-time broadening. For example, hollow semiconductor waveguides, such as the ARROW architecture reported by Yang *et al.* [5] confine atoms across a similar mode area to that of standard HC-PBGF and, thus, exhibit similar linewidths and should display similar saturation powers. On the other hand, evanescent interactions with nanoscale TOF take place on considerably smaller cross-sectional scales and will, thus, yield considerably wider minimum linewidths and much larger saturation intensities. For example, the TOF system reported by Spillane *et al.* [6] experiences a transit-time broadened

lifetime minimum of 110 MHz. This value corresponds to a saturation power of >300 nW. This issue will ultimately impose limitations on the spectroscopic utility of such geometries for sensing applications and resonant nonlinear optics.

C. Impact of increased linewidths on off-resonant applications

The increased homogeneous linewidths associated with effects such as transit-time broadening also strongly impact on the utility of such systems for nonresonant applications. Here, we elucidate the effect by studying its impact on the delay times generated in a passive slow-light experiment. As recently shown by Camacho *et al.* [49] when a short laser pulse is tuned between two strongly absorbing and widely spaced resonances, the amount of group delay experienced by the pulse is inversely proportional to the homogeneous linewidths, and is approximately given by

$$\tau_g = \frac{-\ln(T)}{2\pi\gamma}, \quad (4)$$

where τ_g is the pulse delay, T is the peak pulse transmission, and γ is the homogeneous linewidth of the two resonances. This approximate expression is based on the assumption that the pulse is centered between the two resonances, which are Lorentzians of equivalent strength. It is interesting to note that the achievable time delay does not depend explicitly on the frequency spacing between flanking resonances but rather indirectly via the achievable optical depth at the pulse frequency through the transmission T . For an ~ 2.5 ns pulse centered between the ^{85}Rb D_2 line doublet in a bulk vapor cell, Camacho *et al.* [49] showed that the time delay closely follows Eq. (4), with the expected natural linewidth of 6.07 MHz.

In Fig. 6, we present results of similar passive slow-light experiments conducted in the HC-PBGF on the ^{85}Rb D_1 line in HC-PBGF using 4.6 ns pulses. By fitting the data in Fig. 6 to Eq. (4) illustrates that the transit-time and other broadening mechanisms reduce pulse delay by a factor of 10 in comparison to a bulk cell geometry. From the data in Fig. 6,

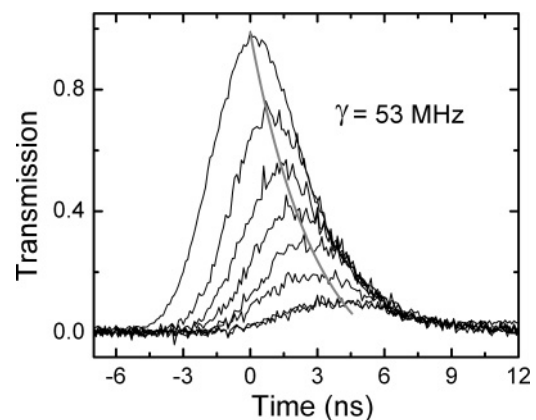


FIG. 6. Passive slow light in the center of the Rb D_1 line. Pulse delay in HC-PBGF as a function of optical depth for a 4.6 ns, 795 nm pulse centered between the ^{85}Rb $F = 2 \rightarrow F' = 2$ and $F = 3 \rightarrow F' = 3$ transitions. The solid gray line is a fit to an exponential function that estimates the experimentally accessed homogeneous linewidth (see text).

we estimate a Lorentzian linewidth of 53 ± 20 MHz, which is slightly broader than that estimated by the more direct means discussed previously. Deviations from ideal behavior are due to the fact that the D_1 line is not composed of an isolated doublet, but rather contains four lines of different strengths, and that as shown previously [33], at this spectral location in the center of the D_1 line, the line shape follows a Voigt profile with a nonnegligible Doppler-broadened Gaussian component. Nonetheless, comparing our pulse-delay results to those reported for bulk cells [45,50] clearly demonstrates that the modifications to the spectroscopic line shapes of atoms confined in waveguiding geometries can also be important for highly nonresonant light-matter interactions.

IV. SUMMARY

We have performed a detailed spectroscopic study of light-matter interactions with warm alkali atoms confined to the $6 \mu\text{m}$ core of a hollow-core photonic band-gap fiber. Using saturable-absorption spectroscopy, we show, for the first time, the various line-shape shifts, broadening, and distortions

that take place in such a system, and further discuss the relevance of these findings to similar micrometer-scale light-atom interaction geometries. We find that the use of a strong desorption beam for the creation of an atomic vapor leads to strong ac Stark shifts, even when detuned off-resonance by many thousands of gigahertz. Furthermore, the Gaussian-like spatial profile of the light modes in these waveguides leads to a distribution of ac Stark shifts and, thus, to considerable line-shape broadening and distortion. These effects can be mitigated by performing the interaction of interest immediately after the desorption beam is turned off. In addition, the effects of transit-time broadening play an important role even for applications based on nonresonant interactions such as slow light and pulse delays.

ACKNOWLEDGMENTS

We gratefully acknowledge financial support from the Centre for Nanoscale Systems, the Air Force Office of Scientific Research, and the Defense Advanced Research Projects Agency under the Slow-Light program.

-
- [1] M. Bajcsy, S. Hofferberth, V. Balic, T. Peyronel, M. Hafezi, A. S. Zibrov, V. Vuletic, and M. D. Lukin, *Phys. Rev. Lett.* **102**, 203902 (2009).
 - [2] P. Londero, V. Venkataraman, A. R. Bhagwat, A. D. Slepko, and A. L. Gaeta, *Phys. Rev. Lett.* **103**, 043602 (2009).
 - [3] F. Benabid, J. C. Knight, G. Antonopoulos, and P. St. J. Russell, *Science* **298**, 399 (2002).
 - [4] S. Ghosh, J. E. Sharping, D. G. Ouzounov, and A. L. Gaeta, *Phys. Rev. Lett.* **94**, 093902 (2005).
 - [5] W. G. Yang, D. B. Conkey, B. Wu, D. L. Yin, A. R. Hawkins, and H. Schmidt, *Nature Photon.* **1**, 331 (2007).
 - [6] S. M. Spillane, G. S. Pati, K. Salit, M. Hall, P. Kumar, R. G. Beausoleil, and M. S. Shahriar, *Phys. Rev. Lett.* **100**, 233602 (2008).
 - [7] M. Wilzbach, D. Heine, S. Groth, X. Liu, T. Raub, B. Hessmo, and J. Schmiedmayer, *Opt. Lett.* **34**, 259 (2009).
 - [8] N. Gayraud, L. W. Kornaszewski, J. M. Stone, J. C. Knight, D. T. Reid, D. P. Hand, and W. N. MacPherson, *Appl. Opt.* **47**, 1269 (2008).
 - [9] F. Couny and F. Benabid, *J. Opt. A, Pure Appl. Opt.* **11**, 103002 (2009).
 - [10] S. Knappe, V. Velichansky, H. G. Robinson, J. Kitching, and L. Hollberg, *Rev. Sci. Instrum.* **74**, 3142 (2003).
 - [11] K. Knabe, W. Shun, J. K. Lim, K. A. Tillman, P. S. Light, F. Couny, N. Wheeler, R. Thapa, A. M. Jones, J. W. Nicholson, B. R. Washburn, F. Benabid, and K. L. Corwin, *Opt. Express* **17**, 16017 (2009).
 - [12] D. A. Braje, V. Balic, G. Y. Yin, and S. E. Harris, *Phys. Rev. A* **68**, 041801(R) (2003).
 - [13] A. M. C. Dawes, L. Illing, S. M. Clark, and D. J. Gauthier, *Science* **308**, 672 (2005).
 - [14] D. F. Phillips, A. Fleischhauer, A. Mair, R. L. Walsworth, and M. D. Lukin, *Phys. Rev. Lett.* **86**, 783 (2001).
 - [15] R. M. Camacho, P. K. Vudyasetu, and J. C. Howell, *Nature Photon.* **3**, 103 (2009).
 - [16] D. G. Ouzounov, F. R. Ahmad, D. Müller, N. Venkataraman, M. T. Gallagher, M. G. Thomas, J. Silcox, K. W. Koch, and A. L. Gaeta, *Science* **301**, 1702 (2003).
 - [17] S. Ghosh, A. R. Bhagwat, C. K. Renshaw, S. Goh, A. L. Gaeta, and B. J. Kirby, *Phys. Rev. Lett.* **97**, 023603 (2006).
 - [18] F. Benabid, P. S. Light, F. Couny, and P. St. J. Russell, *Opt. Express* **13**, 5694 (2005).
 - [19] J. Henningsen, J. Hald, and J. C. Petersen, *Opt. Express* **13**, 10475 (2005).
 - [20] R. Thapa, K. Knabe, M. Faheem, A. Naweed, O. L. Weaver, and K. L. Corwin, *Opt. Lett.* **31**, 2489 (2006).
 - [21] A. M. Cubillas, J. Hald, and J. C. Petersen, *Opt. Express* **16**, 3976 (2008).
 - [22] B. Wu, J. F. Hulbert, A. R. Hawkins, and H. Schmidt, *J. Lightwave Technol.* **26**, 3727 (2008).
 - [23] J. T. Robinson, L. Chen, and M. Lipson, *Opt. Express* **16**, 4296 (2008).
 - [24] S. M. Hendrickson, T. B. Pittman, and J. D. Franson, *J. Opt. Soc. Am. B* **26**, 267 (2009).
 - [25] M. Trupke, E. A. Hinds, S. Eriksson, E. A. Curtis, Z. Moktadir, E. Kukhareuka, and M. Kraft, *Appl. Phys. Lett.* **87**, 211106 (2005).
 - [26] E. A. Hinds, M. Trupke, B. Darquié, J. Goldwin, and G. Dutier, in *Proceedings of the 18th International Conference On Laser Spectroscopy (ICOLS)*, edited by L. Hollberg, J. Bergquist, and M. Kasevich (World Scientific, Singapore, 2008), pp. 272–282.
 - [27] T. Aoki, B. Dayan, E. Wilcut, W. P. Bowen, A. S. Parkins, T. J. Kippenberg, K. J. Vahala, and H. J. Kimble, *Nature (London)* **443**, 671 (2006).
 - [28] B. Dayan, A. S. Parkins, T. Aoki, E. P. Ostby, K. J. Vahala, and H. J. Kimble, *Science* **319**, 1062 (2008).

- [29] A. R. Bhagwat and A. L. Gaeta, *Opt. Express* **16**, 5035 (2008).
- [30] S. Knappe, V. Velichansky, H. G. Robinson, J. Kitching, and L. Hollberg, *Rev. Sci. Instrum.* **74**, 3142 (2003).
- [31] J. Hald, J. C. Petersen, and J. Henningsen, *Phys. Rev. Lett.* **98**, 213902 (2007)
- [32] P. S. Light, F. Benabid, F. Couny, M. Maric, and A. N. Luiten, *Opt. Lett.* **32**, 1323 (2007).
- [33] F. Benabid, F. Couny, J. C. Knight, T. A. Birks, and P. St. J. Russell, *Nature (London)* **434**, 488 (2005).
- [34] A. D. Slepkov, A. R. Bhagwat, V. Venkataraman, P. Londero, and A. L. Gaeta, *Opt. Express* **16**, 18976 (2008).
- [35] A. R. Bhagwat, A. D. Slepkov, V. Venkataraman, P. Londero, and A. L. Gaeta, *Phys. Rev. A* **79**, 063809 (2009).
- [36] C. K. Carniglia, L. Mandel, and K. H. Drexhage, *J. Opt. Soc. Am.* **62**, 479 (1972).
- [37] T. Baehr-Jones, M. Hochberg, C. Walker, and A. Scherer, *Appl. Phys. Lett.* **86**, 081101 (2005).
- [38] J. Henningsen and J. Hald, *Appl. Opt.* **47**, 2790 (2008).
- [39] K.-J. Boller, A. Imamolu, and S. E. Harris, *Phys. Rev. Lett.* **66**, 2593 (1991).
- [40] D. J. Fulton, S. Shepherd, R. R. Moseley, B. D. Sinclair, and M. H. Dunn, *Phys. Rev. A* **52**, 2302 (1995).
- [41] W. Demtröder, *Laser Spectroscopy* (Springer-Verlag, Berlin, 1973).
- [42] A. Gozzini, F. Mango, J. H. Xu, G. Alzetta, F. Maccarrone, and R. A. Bernheim, *Nuovo Cimento D* **15**, 709 (1993).
- [43] D. Lukin and A. Imamoglu, *Nature (London)* **413**, 273 (2001).
- [44] D. A. Steck, ^{87}Rb and ^{85}Rb D_1 line data, [<http://steck.us/alkalidata/>] (2001).
- [45] K. Shimoda, ed., *High-Resolution Laser Spectroscopy*, (Springer-Verlag, New York, 1976).
- [46] S. Haroche and F. Hartmann, *Phys. Rev. A* **6**, 1280 (1972).
- [47] P. St. J. Russell, *J. Lightwave Technol.* **24**, 4729 (2006).
- [48] M. L. Citron, H. R. Gray, C. W. Gabel, and C. R. Stroud Jr., *Phys. Rev. A* **16**, 1507 (1977).
- [49] R. M. Camacho, M. V. Pack, and J. C. Howell, *Phys. Rev. A* **73**, 063812 (2006).
- [50] H. Tanaka, H. Niwa, K. Hayami, S. Furue, K. Nakayama, T. Kohmoto, M. Kunitomo, and Y. Fukuda, *Phys. Rev. A* **68**, 053801 (2003).

All-optical modulation of four-wave mixing in an Rb-filled photonic bandgap fiber

Vivek Venkataraman,^{*,†} Pablo Lonero,[†] Amar R. Bhagwat, Aaron D. Slepko, and Alexander L. Gaeta

School of Applied and Engineering Physics, Cornell University, Ithaca, New York 14853, USA

**Corresponding author: vv49@cornell.edu*

Received April 16, 2010; revised June 4, 2010; accepted June 8, 2010;

posted June 16, 2010 (Doc. ID 127096); published June 30, 2010

We demonstrate efficient all-optical modulation using Rb vapor confined to a hollow-core photonic bandgap fiber. The intensity of a signal field participating in the four-wave-mixing process is modulated using a weak switching field. We observe 3 dB of attenuation in the signal field with only 3600 photons of switching energy, corresponding to 23 photons per atomic cross section $\lambda^2/(2\pi)$. Modulation bandwidths as high as 300 MHz are observed. © 2010 Optical Society of America

OCIS codes: 190.4380, 270.1670.

Nonlinear quantum-optical techniques are being explored to solve problems in optical information processing. A number of schemes for efficient all-optical switches [1–4], all-optical quantum computing gates [5,6], and non-demolition (QND) measurements [7–10] have been either proposed or demonstrated. These approaches require the realization of systems that can achieve measurable nonlinearities at the single-photon level and the development of schemes that can optimally exploit their nonlinear response. Consequently, there is considerable interest in developing media with high optical nonlinearities coupled with tight confinement of the light mode to enhance the intensity. Complementing these efforts are schemes where the frequencies of the interacting light modes and the energy levels of the medium facilitate strong light-matter coupling [2,4,7,10].

Alkali vapors have been used extensively for light-matter interactions due to their large cross section per atom, well-defined energy-level structure, long interaction times, and the large optical depths that can be achieved. Optical waveguides, such as photonic bandgap fibers (PBGFs) with a hollow core, allow an alkali vapor to fill the inside of the guided region and interact with single-mode optical fields. This architecture confines both the atoms and the optical fields transversely to a region that is a few wavelengths in size, which permits weak fields to interact strongly with the atoms over a length that is much larger than the Rayleigh diffraction length. Such systems have been shown to produce strong nonlinearities at ultralow light levels [3,11].

Resonantly enhanced multilevel atomic interactions are attractive for exploiting low-light-level optical phenomena based on quantum interference in alkali atoms. Coherent interactions that exploit narrow resonances have yielded novel nonlinear processes, such as electromagnetically induced transparency [12] and coherent population trapping [13]. For example, in a “lambda” scheme, two optical probe fields couple two ground states of the atom to a single excited state and establish coherence between the two ground states, which results in atom-light states called polaritons. Similar effects can be generated by using a double-lambda scheme, which uses four optical fields to couple the two ground states to an excited state in a four-wave-mixing (FWM) process [14,15]. These polaritons can interact with other external

optical fields and can be used to perturb the atomic ground state coherence resulting in the change in transmission of a probe beam. The external perturbing field, or “switching” field, usually couples one of the ground states to another separate excited state. An on-resonance switching field can be used for low-power all-optical modulation or switching [4], while a slightly off-resonant switching beam can be employed for QND detection schemes [7].

Here we present all-optical intensity modulation of a signal field that is participating in the FWM process with Rb in a hollow-core PBGF. We have previously shown that large optical depths can be generated in a Rb-PBGF system using light-induced atomic desorption [16], which can result in large effective nonlinear susceptibilities and FWM gains greater than 100 with microwatts of pump power [11]. Consequently, introducing a field that can perturb this waveguide-based FWM allows us to study all-optical perturbations of highly nonlinear behavior at extremely low light powers.

The energy-level diagram for our scheme is shown in Fig. 1. We use a double-lambda scheme on the D1 line

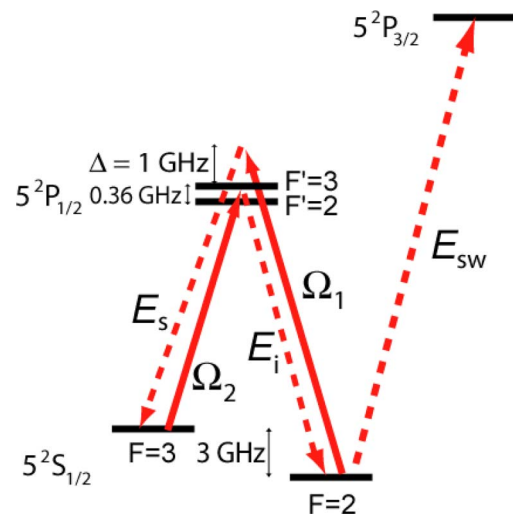


Fig. 1. (Color online) Energy-level diagram of the modulation scheme. FWM is generated in a double-lambda configuration on the D1 ($5^2P_{1/2}$) transition of Rb-85. It is modulated by periodically turning the switching field E_{sw} on to the D2 ($5^2P_{3/2}$) transition.

(795 nm) of Rb-85 to observe FWM with nondegenerate pumps. One pump field Ω_1 is blue detuned by 1 GHz from the $F = 2 \rightarrow F' = 3$ resonance, while the other pump field Ω_2 is tuned between the $F = 3 \rightarrow F' = 2$ and $F = 3 \rightarrow F' = 3$ transitions. A weak signal field E_s blue detuned by 1 GHz from the $F = 3 \rightarrow F' = 3$ transition is also coupled through the PBGF and generates an idler field E_i via the FWM process. The signal is cross polarized with respect to the pump waves, and all three beams are co-propagating in the PBGF. The generated idler is also co-propagating with the same polarization as the signal. The switching field E_{sw} , which is also cross polarized with the pumps, is resonant with the $F = 2$ transition of the D2 line (780 nm) of Rb-85.

Figure 2 shows the experimental setup. We use a 3 cm long PBGF (Crystal Fiber AIR-6-800, 6 μm diameter core) that sits inside a vacuum cell with a Rb source attached [16]. The pump beams are combined with the signal and switching beams by using a polarization beam splitter (PBS) cube at the input of the PBGF, which ensures that the polarizations are orthogonal. A small portion of each input field is sent to a reference Rb vapor cell for frequency calibration. A pulsed desorption beam at 808 nm (detuned far from the Rb-85 resonances), which is coupled counterpropagating to the pump and signal waves, is used to generate the desired vapor density and optical depth in the fiber [17]. The vapor density generated in the fiber is such that, in the presence of the pumps (tens of microwatts in power), the signal experiences a gain of 2 at the two-photon resonance (peak of the FWM gain curve). The switching beam is temporally modulated as a triangle wave, at frequencies from 500 Hz – 1 kHz. The modulated signal exits the fiber, is separated from the pumps by a second PBS and from the idler and switching beams by a temperature-controlled etalon (400 MHz linewidth), and is detected by a photomultiplier tube (PMT).

Figure 3(a) shows the modulated signal at 500 Hz with $\sim 1 \mu\text{W}$ of peak switching power. The input signal power is 5 nW, and its frequency is set exactly at the two-photon resonance so that, at the output of the fiber, the signal power is 10 nW. We see that, in the presence of the switching field, which is modulated at 500 Hz, the signal is attenuated by 50% (3 dB) to 5 nW. The switching field spoils the gain, and the signal passes through the fiber as

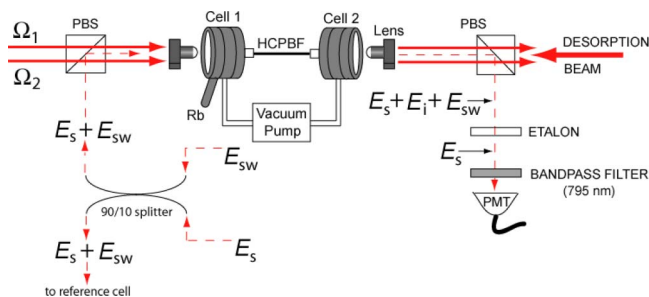


Fig. 2. (Color online) Experimental setup. The switching and signal fields are combined with the pump fields on a PBS. The beams are then focused into the core of the fiber. A counter-propagating desorption beam generates the desired vapor density and optical depth. The modulated signal field is filtered from the pump fields by a second PBS and from the idler and switching fields by an etalon and is then detected with a PMT.

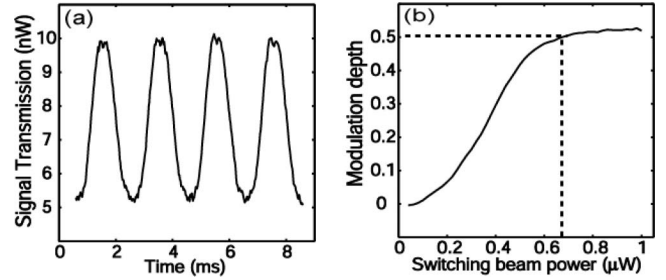


Fig. 3. (a) Modulated signal. FWM modulation at 500 Hz with the signal tuned to the two-photon resonance. The 5 nW signal experiences a gain of 2 with 15 μW of total pump power. We observe 3 dB of attenuation with 1 μW of switching power. (b) Saturation of modulation depth. Signal modulation depth as a function of switching power. Modulation begins to saturate at 0.65 μW .

if there was no FWM, and the idler field is completely extinguished. Figure 3(b) shows the modulation depth observed in the signal as a function of the peak switching power. We find that the modulation depth begins to saturate at 50% for a switching power of 0.65 μW [see dotted line in Fig. 3(b)], and increasing the switching power further does not improve the modulation depth. A slow scan of the signal frequency about two-photon resonance reveals that the modulation is present over the entire FWM gain bandwidth of ~ 100 MHz, which implies a system response time of 1.6 ns. Taking this response time into account, 50% modulation at 0.65 μW of switching power corresponds to 3600 photons of switching energy or to 23 photons per atomic cross section $\lambda^2/(2\pi)$.

We interpret these results as the consequence of the population cycling on the D2 transition that is induced by the switching beam. This spoils the phase relationship between the ground states and destroys their coherence, which is necessary for performing FWM, within one Rabi cycle. The Rabi frequency corresponding to ~ 600 nW of switching power on the D2 line is 120 MHz, i.e., roughly equal to the FWM gain bandwidth. Once there is sufficient power to destroy coherence within the FWM response time, greater switching power no longer increases the amount of modulation, which leads to the saturation behavior seen with respect to switching power.

We also studied the effect of gain/modulation bandwidth B on the modulation depth M for a constant switching field power (see Fig. 4). The FWM gain bandwidth can be modified by changing the relative powers of the two pump fields. In the double-lambda scheme used here, the FWM gain coefficient is proportional to the ratio of the Rabi frequency of the off-resonant pump to that of the on-resonant pump, i.e., to Ω_1/Ω_2 . Since the gain bandwidth is proportional to the product of the Rabi frequencies of the two pumps, i.e., $\Omega_1\Omega_2$ [11,15], one can modify the gain bandwidth without changing the actual gain by simply changing the relative pump powers such that $\Omega_1\Omega_2$ varies but Ω_1/Ω_2 maintains its value. Based on this idea, we observe gain/modulation bandwidths up to 300 MHz. It is evident that the modulation depth decreases with increasing bandwidth for a given switching power (circles). We can determine the number of switching photons required for 3 dB modulation of the signal field, i.e., the switching energy, by calculating the product of the switching power required for 50% modulation

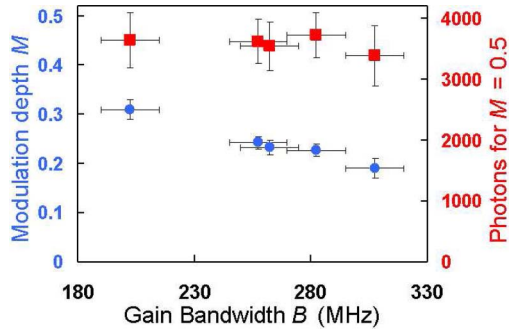


Fig. 4. (Color online) Modulation depth and number of switching photons versus FWM bandwidth. The circles show the modulation depth observed in the signal field as a function of the FWM gain bandwidth. The switching power used for all the measurements was 400 nW. The squares show the switching photon number required for 50% modulation of the signal. The switching photon number is observed to be fairly insensitive to bandwidth. Error bars represent measurement inaccuracy.

($M = 0.5$) and the response time of the system (inverse of the bandwidth), for each bandwidth value B . We see that the number of photons required in the switching field is relatively insensitive to the bandwidth (squares), and the data agree fairly well with the estimated number of 3600 photons.

In summary, we have observed all-optical modulation of FWM using Rb vapor in a PBGF. We observe 3 dB attenuation of the signal beam using only 3600 photons of switching energy or 23 photons per atomic cross section $\lambda^2/(2\pi)$, which is comparable to that achieved in more elaborate cold atom setups [2,3]. Moreover, we demonstrate tunable modulation bandwidths of up to 300 MHz, which is very high for an alkali vapor interaction. These preliminary results show the potential of an Rb-PBGF system for nonlinear optical interactions at a low photon number. For example, it should be possible to enhance important alkali-based quantum-optical interactions, such as QND measurement techniques and the production of squeezed states, due to the tight confinement and high optical depths. One limiting factor in our setup currently is the small transit time (~ 5 ns) of the Rb atoms across the core of the PBGF, which limits the ground state coherence time. Producing a purer state among the ground hyperfine levels by increasing the transit time through collisions with a buffer gas should improve the

results [18–20]. One could also increase the available switching bandwidth by broadening the D2 transition with the injection of a buffer gas into the system.

The authors gratefully acknowledge financial support from the National Science Foundation (NSF), the U.S. Army Research Office (USARO), and the U.S. Air Force Office for Scientific Research (USAFOSR).

[†]These authors contributed equally to this work.

References

1. A. M. C. Dawes, L. Illing, S. M. Clark, and D. J. Gauthier, *Science* **308**, 672 (2005).
2. D. A. Braje, V. Balic, G. Y. Yin, and S. E. Harris, *Phys. Rev. A* **68**, 041801 (R) (2003).
3. M. Bajcsy, S. Hofferberth, V. Balic, T. Peyronel, M. Hafezi, A. S. Zibrov, V. Vuletic, and M. D. Lukin, *Phys. Rev. Lett.* **102**, 203902 (2009).
4. S. E. Harris and Y. Yamamoto, *Phys. Rev. Lett.* **81**, 3611 (1998).
5. P. Kok, W. J. Munro, K. Nemoto, T. C. Ralph, J. P. Dowling, and G. J. Milburn, *Rev. Mod. Phys.* **79**, 135 (2007).
6. J. D. Franson, B. C. Jacobs, and T. B. Pittman, *Phys. Rev. A* **70**, 062302 (2004).
7. H. Schmidt and A. Imamoglu, *Opt. Lett.* **21**, 1936 (1996).
8. N. Matsuda, R. Shimizu, Y. Mitsumori, H. Kosaka, and K. Edamatsu, *Nat. Photon.* **3**, 95 (2009).
9. P. Grangier, J. F. Roch, and G. Roger, *Phys. Rev. Lett.* **66**, 1418 (1991).
10. H. Kang and Y. Zhu, *Phys. Rev. Lett.* **91**, 093601 (2003).
11. P. Londero, V. Venkataraman, A. R. Bhagwat, A. D. Slepko, and A. L. Gaeta, *Phys. Rev. Lett.* **103**, 043602 (2009).
12. J. E. Field, K. H. Hahn, and S. E. Harris, *Phys. Rev. Lett.* **67**, 3062 (1991).
13. B. J. Dalton, R. McDuff, and P. L. Knight, *J. Mod. Opt.* **32**, 61 (1985).
14. M. D. Lukin, A. B. Matsko, M. Fleischhauer, and M. O. Scully, *Phys. Rev. Lett.* **82**, 1847 (1999).
15. A. Andre, “Nonclassical states of light and atomic ensembles,” Ph.D. dissertation (Harvard University, 2005).
16. A. D. Slepko, A. R. Bhagwat, V. Venkataraman, P. Londero, and A. L. Gaeta, *Opt. Express* **16**, 18976 (2008).
17. A. R. Bhagwat, A. D. Slepko, V. Venkataraman, P. Londero, and A. L. Gaeta, *Phys. Rev. A* **79**, 063809 (2009).
18. W. Happer, *Rev. Mod. Phys.* **44**, 169 (1972).
19. M. Erhard and H. Helm, *Phys. Rev. A* **63**, 043813 (2001).
20. M. M. Hossain, S. Mitra, B. Ray, and P. N. Ghosh, *Laser Phys.* **19**, 2008 (2009).

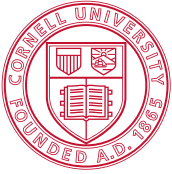
VOLUME I: TECHNICAL PROPOSAL

1. BAA 08-22: Defense Sciences Research and Technology
2. *Technical Area:* Slow light
3. *Lead Organization:* Cornell University
4. *Type of Business:* Other Educational
5. *Contractor's Reference Number:* N/A
6. *Team Members:* University of Southern California
7. *Proposal Title:* **Large Tunable Delays in Fiber and On-Chip via Conversion/Dispersion**
8. *Technical POC:*
Professor Alexander Gaeta
School of Applied & Engineering Physics
Cornell University
Ithaca, NY 14853
Tel: (607) 255-9983 Fax: (607) 255-7658
e-mail: a.gaeta@cornell.edu
9. *Administrative POC:*
Ms. Diane West
Grant & Contract Officer
373 Pine Tree Rd.
Cornell University
Ithaca, NY 14850
Tel: (607) 255-0655 Fax: (607) 255-5058
e-mail: dw68@cornell.edu
10. *Date Prepared:* May 29, 2008
11. *Total Proposed Cost:* \$2,300,000

LARGE TUNABLE DELAYS IN FIBER AND ON-CHIP VIA CONVERSION/DISPERSION

CONTENTS

I.B. OFFICIAL TRANSMITTAL LETTER.....	3
II.A. EXECUTIVE SUMMARY	4
II.B. PROPOSED RESEARCH AND DEVELOPMENT.....	5
II.B.1. OVERVIEW AND RATIONALE.....	5
II.B.2. PROPOSED RESEARCH.....	6
<i>II.B.2.1 Maximization of Delay</i>	<i>6</i>
<i>II.B.2.2 Using PIN Structures to Increase FWM Efficiency</i>	<i>8</i>
<i>II.B.2.3 Fabrication of long, low-loss waveguides for the dispersive element</i>	<i>9</i>
<i>II.B.2.4 Integration of the FWM and Dispersive Elements</i>	<i>9</i>
<i>II.B.2.5 System Applications of Conversion/Dispersion</i>	<i>10</i>
II.C.1. MILESTONES.....	13
II.D. STATEMENT OF WORK.....	14
II.E. MANAGEMENT PLAN.....	15
III.A. INTELLECTUAL PROPERTY	15
III.A.1. PATENTS.....	15
IV. ADDITIONAL INFORMATION	16
IV.1 BIBLIOGRAPHY.....	16



Cornell University
Office of Sponsored Programs

Cornell University
373 Pine Tree Road
Ithaca, NY 14850

Telephone: 607 255-5014
Fax: 607 255-5058
Web: www.osp.cornell.edu

June 27, 2008

DARPA/DSO
Attn: BAA 08-22
3701 North Fairfax Drive
Arlington, VA 22203-1714

Dear Madam/Sir:

Cornell University is pleased to submit a proposal for Professor Alexander Gaeta in the School of Applied and Engineering Physics.

Cornell University reserves the right to negotiate the terms and conditions of any definitive Contract/Grant which may result from this proposal application. The following link provides the general framework for establishing a sponsored research agreement between Cornell University and entities seeking to support research projects or programs:

http://www.osp.cornell.edu/Policies/Std_Agmt_Terms.html.

In offering to participate in this research program, the participating institution certifies that: neither it nor its principal are presently debarred, suspended, proposed for debarment, declared ineligible, or voluntarily excluded from receiving funds from any Federal department or agency; it is not delinquent on any Federal debt; it is in compliance with the Drug Free Workplace Act of 1988; it is in compliance with 42 CFR part 50 (Objectively in Research) regarding financial conflict-of-interest; no Lobbying was performed with regard to proposal listed above; and assurances are on file for; Misconduct in Science, Civil Rights, Handicapped Individuals, Sex Discrimination and Age Discrimination.

Any correspondence should be sent to my attention and resulting award should be made in the legal name of Cornell University and sent to Office of Sponsored Programs, Cornell University, 373 Pine Tree Road, Ithaca, NY 14850-2820, Phone: (607) 255-5014, Fax: (607) 255-5058, E-mail: cu_awds@cornell.edu, Web: <http://www.osp.cornell.edu>.

We look forward to working with you in the near future.

Sincerely,

A handwritten signature in black ink that reads "Tammy J. Custer". The signature is written in a cursive style.

Tammy J. Custer
Grant and Contract Officer/eRA Specialist
tjb3@cornell.edu

II.A. EXECUTIVE SUMMARY

Our recent work on the use of wavelength conversion and dispersive propagation to produce large tunable delays shows great promise for applications that require information to be buffered. In Phase III of the DARPA/DSO slow light program, we propose to extend our work in conversion/dispersion slow light. Our approach will be transparent to OOK and DPSK modulation formats. The frequency conversion will be performed via broadband four-wave mixing (FWM) in Si nanowaveguides. We will develop two different dispersive delay components that are based on optical fiber or on Si waveguides, which will allow us to pursue a communication systems demonstration as well as demonstrating the fundamental ability to achieve significantly longer optical delays than previously achieved in both fiber-based or chip-based systems.

II.B. PROPOSED RESEARCH AND DEVELOPMENT

II.B.1. OVERVIEW AND RATIONALE

The generation of tunable optical delays has been an area of extensive research over the past decade. The technique that has received the most attention uses the concept of slow light, which takes advantage of the rapidly varying refractive index that accompanies a laser-induced resonance. However, the maximum delay that can be achieved from a slow-light-based tunable delay line is limited by what is known as the delay-bandwidth product [1], which exists since slow light takes advantage of a resonance feature. The delay that can be achieved without pulse distortion is limited by two factors [2]. The first is group-velocity dispersion (GVD) within the resonance feature. Different frequency components of the pulse experience different delays, leading to pulse spreading. The second is the spectral reshaping of the pulse from propagating through the resonance feature. Since the gain or transparency feature is frequency dependent, the spectral shape is not preserved during propagation. An alternative technique for generating larger delays involves using wavelength conversion and dispersion, which takes advantage of GVD in an optical fiber to generate the wavelength-dependent delay [3-6]. The center wavelength of the input signal is shifted and injected into a medium with a large GVD, which yields a delay with respect to the initial, unshifted pulse. A second wavelength converter can then be used to return the signal wavelength to the original wavelength. The total delay is simply a product of the GVD parameter D , the length of the dispersive fiber L_d , and the wavelength shift $\Delta\lambda$. Thus to achieve large delays using this scheme, it is necessary to produce a large wavelength shift and/or large a GVD. Several conversion-dispersion delay schemes have been demonstrated, including soliton self-frequency shift [7], $\chi^{(2)}$ parametric mixing [8,9], four-wave mixing [10-12], cross-absorption modulation [13], cross-polarization modulation [14], and self-phase modulation [15-17], and tunable delays as large as 105 ns have been demonstrated [9]. Many of these schemes depend on the switching speed of the pump laser wavelength. Recently, wavelength switching times < 2 ns have been demonstrated using a Fabry-Perot laser design [18].

In silicon, the proximity of the band edge to the communications band near 1.5 μm results in a bulk contribution to the dispersion in the telecommunication regime that is very large and normal. Nevertheless, using waveguides with ultra-high-degree of confinement, the waveguide contribution to the dispersion can overcome the large normal contribution of the bulk material. Recently, we demonstrated wavelength conversion over a large bandwidth using four-wave mixing (FWM) in Si nanowaveguides [19]. The silicon-on-insulator (SOI) platform is in many ways ideal for nonlinear interactions due to the high index contrast between the silicon core and silica cladding, which allows for strong optical confinement and large effective optical nonlinearities, since the nonlinear coefficient is 200 times larger in silicon than in silica glass. Furthermore, the dispersion in the silicon waveguides can be tailored by controlling the size and shape of the waveguides, and anomalous dispersion can be produced within a small range of waveguide dimensions [20]. Foster *et al.* [21] demonstrated FWM gain of 5.2 dB in silicon

waveguides using a pulsed pump. Recently, the FWM bandwidths have been extended to well over 100 nm in Si waveguides [19], which can be attributed to the short interaction length and dispersion tailoring to operate the pump near the zero-GVD point [20]. This broad bandwidth allows for much larger delays as compared to the previous demonstration of the FWM conversion-dispersion scheme in an optical fiber [10]. Another advantage of the silicon platform is that a cw pump can be used without being phase modulated since in the silicon waveguides the effects of stimulated Brillouin scattering appear to be negligible.

II.B.2. PROPOSED RESEARCH

In the following sections, we describe our proposed ambitious program in which we will use FWM in Si nanowaveguides to demonstrate large tunable delays via conversion/dispersion at far higher bit rates than has been previously demonstrated and for communication system applications. Very large delays at the packet level will be achieved using fiber-based dispersive elements. In addition, we will develop a highly compact integrated tunable delay module in which the FWM and dispersive delay elements reside entirely on the same Si chip.

II.B.2.1 Maximization of Delay

The maximum achievable delay in the conversion-dispersion scheme can be extended by increasing the FWM conversion bandwidth and/or by increasing the length of the dispersive fiber used in the delay stage. However, as a result of dispersive broadening of the pulse, a limit exists on the maximum length of the dispersive fiber that can be used without additional compensating elements. Dispersion compensators, such as chirped fiber Bragg gratings, can be implemented to extend the allowable GVD in the dispersive fiber [8]. In this case, the GVD in the dispersion compensator must be tailored such that it has the same magnitude and the opposite sign as the GVD in the dispersive fiber. Here, we propose a simpler technique that overcomes the GVD-induced pulse broadening by using the inherent temporal phase conjugation associated with FWM, which allows us to further extend the maximum achievable delay.

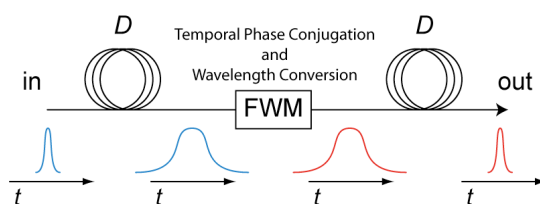


Fig. 1. Delay generator using wavelength conversion and temporal phase conjugation via FWM and two dispersion links. The FWM stage acts both as a wavelength converter and a temporal phase conjugator.

Temporal phase conjugation (TPC) results in the generated field being the complex conjugate of the input field, which results in phase reversal. Thus, implementation of TPC in between two dispersive fiber links results in cancellation of the even-order dispersion contributions. Our delay scheme consists of three stages, the first is a dispersive fiber with dispersion $+D$, the second is a FWM wavelength conversion and phase conjugation stage, and the third is a dispersive fiber with dispersion $+D$, which is responsible for both dispersive delay and dispersion (GVD) dispersion compensation (Fig. 1). For fixed wavelength operation, a second FWM stage is added for wavelength reconversion. The maximum achievable delay is limited by the third-order dispersion (TOD) and the residual second-order dispersion from the wavelength shift that accompanies the TPC in the FWM process. Figure 2 shows the maximum achievable delay and the corresponding dispersion for the parametric mixing and phase conjugation delay scheme. The solid blue line represents the delay that can be achieved without compensation of TOD and the residual second-order dispersion due to the wavelength shift. We assume RZ pulses with a Gaussian profile and a wavelength conversion bandwidth of 70 nm. For 10-Gbit/s data rates, it is possible to achieve 1 μ s of delay without compensation of the residual dispersion. For 40-Gbit/s data, 83 ns of tunable delay can be achieved without compensation of residual dispersion. This delay can be extended with the use of NRZ format input data due to the fact that NRZ signals are more bandwidth-efficient. To achieve larger delays at higher data rates, compensation of the residual dispersion is necessary. With dispersion compensation and larger wavelength conversion bandwidths, tunable delays well over 100 ns can be realized. The dashed red line represents the delay that can be achieved without compensation of TOD.

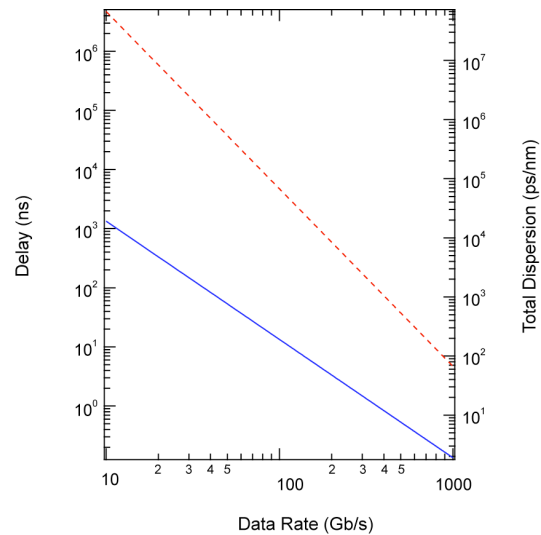


Fig. 2. Maximum delay (right axis) and the magnitude of the allowable dispersion (left axis) as a function of input data rate. We assume RZ pulses with a 33% fill-factor as our input and a wavelength conversion bandwidth of 70 nm. The dashed red line shows the achievable delay if TOD compensation is not performed, and the solid blue line shows achievable delay without residual second-order dispersion and TOD compensation.

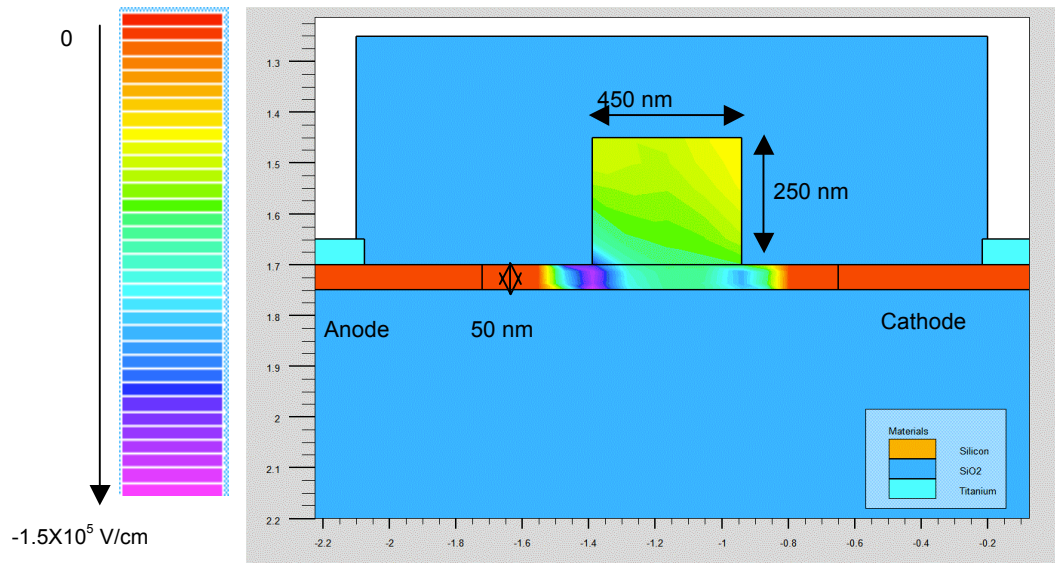


Fig. 3. Extraction electric field under a 5 V reverse bias. The electric field at the center of the rib is close to the value required for theoretical maximum drift speed of carriers.

II.B.2.2 USING PIN STRUCTURES TO INCREASE FWM EFFICIENCY

A key aspect of our system is to improve the FWM efficiency in order to minimize losses and the need for external amplification of the signal after it has been delayed. The primary limitation of the FWM efficiency in Si nanowaveguides is due to the creation of free-carrier absorption (FCA) due to carriers that are created via two-photon absorption of the pump wave. The effects of FCA can be mitigated by reducing the free-carrier lifetime in the Si nanowaveguides, and the lifetime can be reduced by placing the waveguides within a PIN structure and applying an electrical bias to extract the generated free carriers (see Fig. 3). We have shown that the carrier lifetime in ring resonators without a PIN junction is approximately 1 ns. In contrast, when a reverse bias is applied to a ring resonator using a PIN diode, the carriers can be swept out of the ring resonator in less than 20 ps.

We will design the structures so that the PIN junction does not perturb the optical mode (to minimize losses) while still enabling fast carrier extraction. Our preliminary simulations show that with this approach one can achieve the theoretical maximum drift speed of carriers of 10 ps in silicon. Figure 3 shows the distribution of the reverse bias electric field component towards

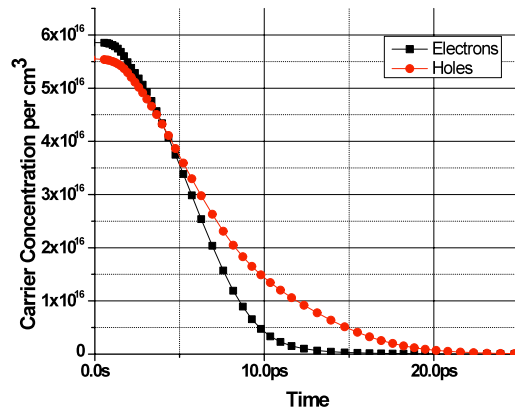


Fig. 4. Simulated concentration of hole and electrons in the center of the waveguide under 5 V reverse bias.

the anode, along the cross section of the waveguide. A reverse bias of -5 V is assumed across a PIN junction built around a waveguide of dimensions 450×250 nm. The waveguides we will implement are slightly larger, but we expect to achieve similar reduction in the free-carrier lifetime. A careful examination of this electric field distribution reveals that charge carriers will be efficiently swept out, as detailed in Fig. 4 in which for the application of a 5 V reverse bias the simulated concentrations of electrons and holes in the center of the rib waveguide are plotted. We expect to achieve even faster extraction responses by optimizing the geometry of the waveguide and the embedded PIN junction.

II.B.2.3. FABRICATION OF LONG, LOW-LOSS WAVEGUIDES FOR THE DISPERSIVE ELEMENTS

Production of relatively long delays in a completely chip-based delay module requires the fabrication of long waveguides on chip of lengths greater than 1 meter. The propagation losses of current silicon waveguides (1.5-3 dB/cm) result mainly from scattering and absorption of the Si/SiO₂ sidewalls of the waveguides caused by the fabrication process which forms the waveguides and these losses must be substantially reduced to levels < 0.2 dB/cm in order to create usable dispersive delay lines. We will address this issue using two main techniques. The first technique consists of the reflow of the exposed resist by heating the sample and therefore removing imperfections at the edges of the resist. We estimate that the losses of the waveguides will be reduced below 0.5 dB/cm. A further reduction in losses will be accomplished by minimizing absorption due to the surface states. We will use a technique for passivating the surfaces. This technique can be done in conjunction with the resist reflow method and involves a cyclic use of a Piranha solution, which slightly oxidizes the exposed surfaces of the etched waveguides and devices, and an HF dip, which removes this oxidation.

II.B.2.4 INTEGRATION OF THE FWM AND DISPERSIVE ELEMENTS

In order to produce a module that resides entirely on a single chip, it is necessary to integrate the FWM and dispersive elements. However, the dimensions of the waveguides for the dispersive element and for the FWM device are very different. We will design coupling regions between the two devices in order to ensure that the modes match and insertion losses are minimized. In order to achieve mode matching we will make use of nanotapers for mode delocalization. The micrometer-long nanotaper coupler that converts *both* the mode size and the effective index of a nm-sized waveguide to that of a much larger waveguide (i.e., the dispersive element). The nanotaper

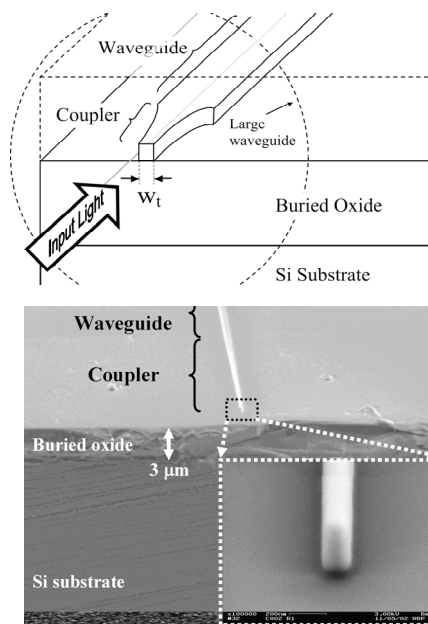


Fig. 5. (top) Schematic of a waveguide with a coupler. (bottom) Scanning electron micrograph of the coupler tip.

consists of a highly confining waveguide tapered to a nanometer-sized tip at the facet, in contact with a larger waveguide [Fig. 5 (top)]. At the tip of width w_t , due to the sub-wavelength dimensions of the tip, the field profile expands inducing a very large mode similar in effective index and profile to that of the large waveguide.

Our simulations show that the coupling losses of the proposed device between a waveguide with a mode diameter of $0.5\ \mu\text{m}$ to the one with a diameter of $5\ \mu\text{m}$ can be as low as 0.5 dB for TE-like mode at $\lambda_0 = 1550\ \text{nm}$ with tip width $w_t = 50\ \text{nm}$. Figure 5 (bottom) shows an angled view of the waveguide and coupler. The inset shows the cross section of the coupler at the tip facet. The structure was fabricated using e-beam lithography and reactive-ion etching. The preliminary results demonstrate the principle of mode delocalization using high confinement waveguides tapered to nm sizes for bridging between optical structures across size scales.

II.B.2.5 SYSTEM APPLICATIONS OF CONVERSION/DISPERSION

We will use the silicon waveguides developed by the Cornell Team to demonstrate communication system applications of conversion/dispersion enabled delay as well as demonstrating the ability to achieve delays with higher bit rates (see Fig. 6). Specifically, we will:

- (i) demonstrate a tunable optical buffer with a maximum buffer depth of 10 packets, a bit rate of 40 Gb/s, and a packet guard time of 1 nanosecond;
- (ii) perform bit-level synchronization and multiplexing of two 20-Gbit/s signals into a single higher bit-rate 40-Gb/s signal;
- (iii) demonstrate variable packet lengths and bit rates via tunable optical delays that will accommodate a dynamically reconfigurable and heterogeneous optical network;
- (iv) achieve delays of 100 ns for a 100-Gb/s channel.

The basic building blocks of our tunable delay approach include:

- a) *Wavelength Conversion*: Wavelength conversion will be achieved by broadband four-wave mixing (FWM) in silicon waveguides.

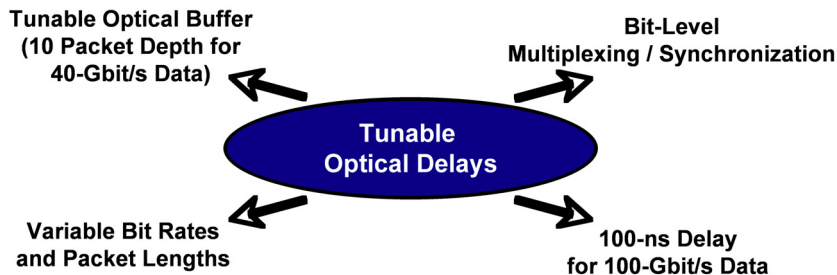


Fig 6. Proposed system applications of continuously tunable optical delays.

- b) *Inter-channel Chromatic Dispersion*: We will use two different types of highly dispersive elements to achieve the wavelength-dependent delay, either: (i) commercially available

dispersion compensating fiber (DCF), or (ii) silicon waveguides. The data signal will be converted back to the original wavelength following the dispersive element.

- c) *Intra-channel Dispersion Compensation*: The intra-channel data degradation produced by the inter-channel dispersion will be compensated by using a narrowband dispersive element of the opposite dispersion sign than that of the original delay-inducing element. This compensator can be a chirped fiber Bragg grating (FBG), will be placed after the wavelength reconversion stage, and will be tunable to accommodate different amounts of shift/delay.

Our specific milestones for Slow Light Phase III include:

(i) Optical Buffer: One data packet (53 bytes) in a 40 Gbit/s stream will be delayed up to 116 ns and will be inserted into an open packet slot (see Fig. 7). A 1-ns guard time will be used between the packets. A reconfiguration time of 1 ns will be achieved by a 10x1 fast optical switch that will switch between the pump wavelengths for the required delay. The clocked pump will convert only the packet to be delayed to the necessary wavelength. Simultaneously, the buffered packet will be erased from the original data stream via an optical modulator driven by a corresponding RF signal. Following the required delay, the packet will be multiplexed with the original data stream. The packet will thus be inserted into its new time slot. The optical buffer will accommodate both on-off-keying (OOK) and differential-phase-shift-keying (DPSK) data modulation formats. To accommodate forward-error-correction (FEC) coding, the bit rate can vary from 40 to 43 Gbit/s. Although the demonstration will be for a single input wavelength, we will show the feasibility of scaling to many input wavelengths.

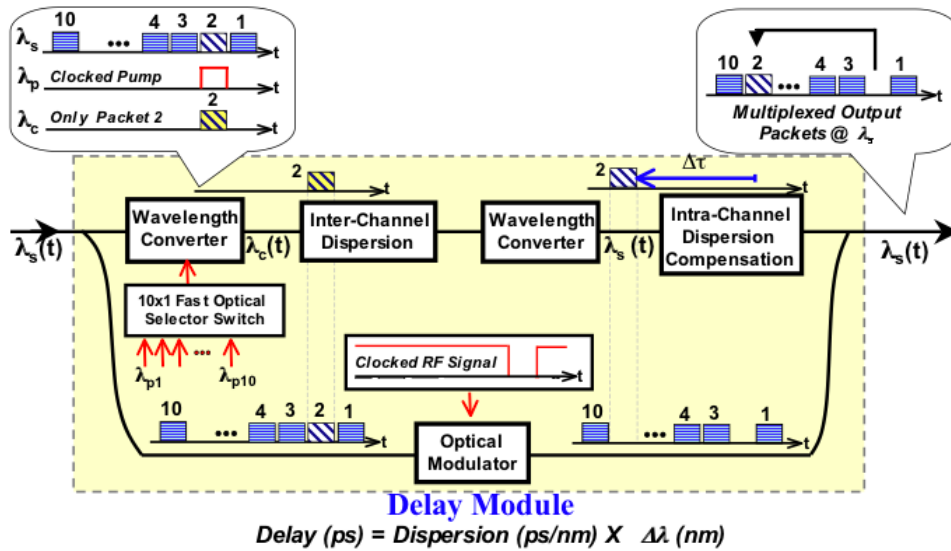


Fig. 7. Schematic of the proposed tunable optical buffer with ns reconfiguration time and a depth of 10 packets.

(ii) Bit-level Multiplexing: On the bit level, two 20-Gbit/s data streams will be seamlessly multiplexed into a single 40-Gbit/s stream (see Fig. 8). One of the streams will be finely and accurately delayed with respect to the second stream, and these two streams will then be multiplexed together.

(iii) Variable Bit Rates and Packet Lengths: The design of the delay module will accommodate variable packet lengths through modification of the driving RF signals. We will demonstrate an optical buffer that will accommodate variable bit rates and/or packet lengths to

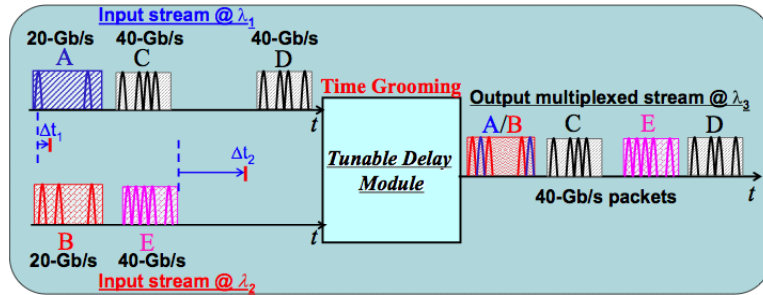


Fig. 8. Illustration of bit-level and packet-level synchronization and multiplexing.

achieve enhanced flexibility and heterogeneity within the network. The bit rate of the input packet streams can range from 10-Gbit/s to 40-Gbit/s.

(iv) High Data Rates: We will demonstrate the tunable delay module for a 100-Gbit/s data stream and achieve delays up to 100 ns. Residual dispersion effects will be carefully assessed and necessary higher-order dispersion compensation will be demonstrated.

I.C.1. MILESTONES

The tables summarizing our milestones and timelines for our fiber and chip-based systems are given below.

Fiber-Based Dispersive Element	6 month	12 month	18 month
FWM efficiency across full bandwidth	-20 dB	-15 dB	-15 dB
Total tunable delay at 40 Gb/s	42.4	63.6	116
Buffer Depth	3	5	10
Chip-Based Dispersive Element			
Loss	1 dB/cm	0.3 dB/cm	0.1 dB/cm
Total tunable delay at 40 Gb/s	50 ps	0.5 ns	5 ns

Both systems will be tested with OOK and DPSK formats, and packets of 53 bytes will be randomly selected for buffering. In addition, to accommodate forward error correction, the bit rate and buffer time will be varied from 40 to 43 Gbit/s.

II.D. STATEMENT OF WORK

In Phase III of the DARPA/DSO slow light program, we propose to extend our work in conversion/dispersion slow light. Our approach uses wavelength conversion, chromatic dispersion, wavelength-re-conversion, and dispersion compensation and will be transparent to OOK and DPSK modulation formats. The frequency conversion will be performed via broadband four-wave mixing (FWM) in Si nanowaveguides. We will develop two different dispersive delay components that are based on optical fiber or on Si waveguides, which will allow us to pursue a communication systems demonstration as well as demonstrating the fundamental ability to achieve significantly longer optical delays than previously achieved in both fiber-based or chip-based systems.

Task 1: Fabricate Si nanowaveguide structures designed to achieve efficient, broadband frequency conversion and optimized to produce large tunable delays for fiber-based and for chip-based dispersive-delay lines. PIN structures will be incorporated into the waveguide elements in order to reduce the free-carrier lifetime and thus increase the overall efficiency of frequency conversion to values greater than -15 dB over the full bandwidth.

Task 2: We will employ the conversion/dispersion method using fiber-based delays to demonstrate widely tunable delays up to 116-ns delays for a 40 Gbit/s data channel which can accommodate a 53-byte packet.

Task 3: Using conversion/dispersion, we will demonstrate time synchronization, multiplexing, and wavelength conversion of two input data channels. Using the same module, we will perform bit-level and packet-level functions: (a) bit: two 20-Gbit/s channels multiplexed onto a single 40-Gbit/s channel, and (b) packet: delay a 40-Gbit/s data packet and insert it into an open packet slot. The functions will also be performed at variable bit rates.

Task 4: We will design and fabricate a dispersive delay line on a Si chip to achieve a total dispersion of 10 ps/nm. Extensive effort will be devoted to create waveguides of lengths up to 10 m with low losses (< 0.2 dB/cm), which will be confined to a chip of area < 40 cm².

Task 5: Fabricate a tunable delay device that resides entirely on a single chip. The dispersive delay lines will be integrated with the FWM nanowaveguides and any other elements (i.e., filters, dispersion compensators) to achieve total delays of 5 ns. We will fabricate and demonstrate the

wavelength scalability of the device by showing that it can be made to operate with 2 wavelengths on 2 different inputs channels.

Task 6: We will perform dispersion compensation in the fiber-based scheme using both commercially-available tunable modules as well as a double-pass approach, in which the effects of dispersion are mostly undone during a phase conjugation associated with the FWM process and reverse pass through the dispersive element. The latter approach will also be applied to the chip-based scheme in addition to the creation of integrated dispersion compensating components.

II.E. MANAGEMENT PLAN

This proposed program will be organized under the rules of the Cornell University and will be led by Professor Alexander Gaeta. Professor Gaeta will have authority to make budgetary decisions for the program and will be responsible for coordinating all aspects of the research effort to ensure progress toward the program goals. He will also be responsible for coordinating, generating and submitting the required technical reports in a timely fashion. Monthly phone conferences will be held between the Cornell and USC groups and graduate students from each university will devote time and effort at the other in an effort to better coordinate and achieve the tasks and milestones. Cornell University's Office of Sponsored Programs will be responsible for establishing and maintaining the program in accordance with all applicable federal and state regulations.

III.A. INTELLECTUAL PROPERTY

No restrictions are intended.

III.A.1. PATENTS

Gaeta has filed a provisional patent entitled "All-Optical Controllable Pulse Delay Generator Using Wavelength Conversion" on 3/19/06, and the application number is 11/377,921. In addition, Gaeta and Lipson filed a provisional patent last year entitled "Silicon integrated photonic parametric amplifier, oscillator, and wavelength converter", which was filed on 3/26/07 and the application number is 60/908,002. We expect that additional related intellectual property will be developed under this proposal.

IV. ADDITIONAL INFORMATION

IV.1 BIBLIOGRAPHY

1. R. W. Boyd, D. J. Gauthier, and A. L. Gaeta, "Applications of slow light in telecommunications," *Opt. Photon. News* **17**, 18–22 (2006).
2. R. W. Boyd, D. J. Gauthier, A. L. Gaeta, and A. E. Willner, "Maximum time delay achievable on propagation through a slow-light medium," *Phys. Rev. A* **72**, 023801 (2005).
3. M. Burzio, P. Cinato, R. Finotti, P. Gambini, M. Puleo, E. Vezzoni, and L. Zucchelli, "Optical cell synchronization in an ATM optical switch," in *Proc. ECOC '94*, Florence, Italy, 2, 581–584 (1994).
4. L. Zucchelli, M. Burzio, and P. Gambini, "New solutions for optical packet delineation and synchronization in optical packet switched networks," in *Proc. ECOC '96*, Oslo, Norway, 3, 301–304 (1996).
5. K. Shimizu, G. Kalogerakis, K. Wong, M. Marhic, and L. Kazovsky, "Timing jitter and amplitude noise reduction by a chirped pulsed-pump fiber OPA," in *Proc. OFC '03*, Anaheim, USA, 1, 197–198 (2003).
6. J. van Howe and C. Xu, "Ultrafast optical delay line using soliton propagation between a time-prism pair," *Opt. Express* **13**, 1138–1143 (2005).
7. S. Oda and A. Maruta, "All-optical tunable delay line based on soliton self-frequency shift and filtering broadened spectrum due to self-phase modulation," *Opt. Express* **14**, 7895–7902 (2006).
8. Y. Wang, C. Yu, L. Yan, A. E. Willner, R. Roussev, C. Langrock, M. M. Fejer, J. E. Sharping, and A. E. Gaeta, "44-ns continuously tunable dispersionless optical delay element using a PPLN waveguide with two-pump configuration, DCF, and a dispersion compensator," *Photon. Technol. Lett.* **19**, 861–863 (2007).
9. L. C. Christen, I. Fazal, O. Yilmaz, X. Wu, S. R. Nuccio, A. E. Willner, C. Langrock, and M. Fejer, "Tunable 105-ns optical delay for 80-Gb/s RZ-DQPSK, 40-Gbit/s RZ-DPSK, and 40-Gbit/s RZ-OOK signals using wavelength conversion and chromatic dispersion," *Optical Fiber Communication Conference*, paper OTuD1 (2008).
10. J. E. Sharping, Y. Okawachi, J. van Howe, C. Xu, Y. Wang, A. E. Willner, and A. L. Gaeta, "All-optical, wavelength and bandwidth preserving, pulse delay based on parametric wavelength conversion and dispersion," *Opt. Express* **13**, 7872–7877 (2005).
11. J. Ren, N. Alic, E. Myslivets, R. E. Saperstein, C. J. McKinstrie, R. M. Jopson, A. H. Gnauck, P. A. Andrekson, and S. Radic, "12.47 ns continuously-tunable two-pump parametric delay," *European Conference on Optical Communications*, paper Th4.4.3 (2006).
12. M. P. Fok and C. Shu, "Tunable optical delay using four-wave mixing in a 35-cm highly nonlinear bismuth-oxide fiber and group velocity dispersion," *J. Lightwave Technol.* **26**, 499–504 (2008).

13. M. P. Fok and C. Shu, "Tunable optical delay with signal regeneration using cross-absorption modulation wavelength conversion and chromatic dispersion," in Proc. CLEO/QELS '08, San Jose, CA, USA, CThH4 (2008).
14. B. P. P. Kuo, P. C. Chui, and K. K. Y. Wong, "Simultaneous optical delay and NRZ-RZ format conversion via cross-polarization modulation and pulse pre-chirping," in Proc. CLEO/QELS '08, San Jose, CA, USA, CThH5 (2008).
15. Y. Okawachi, J. E. Sharping, C. Xu, and A. L. Gaeta, "Large tunable optical delays via self-phase modulation and dispersion," *Opt. Express* **14**, 12022–12027 (2006).
16. Z. Hu and D. J. Blumenthal, "SPM-based 2R regenerative 10Gbps optically linearly controlled delay line with 0ps to 170 ps tuning range," in Proc. OFC '07, Anaheim, USA, OME4 (2007).
17. Y. Okawachi, R. Salem, and A. L. Gaeta, "Continuous tunable delays at 10-Gb/s data rates using self-phase modulation and dispersion," *J. Lightwave Technol.* **25**, 3710–3715 (2007).
18. C. Yeh, C. Lee, and S. Chi, "Fast wavelength switching based on a Fabry-Perot laser pair using optical injection," *Jap. J. Appl. Phys.* **43**, 3454-3455 (2004).
19. M. A. Foster, A. C. Turner, R. Salem, M. Lipson, and A. L. Gaeta, "Broad-band continuous-wave parametric wavelength conversion in silicon nanowaveguides," *Opt. Express* **15**, 949–12,958 (2007).
20. A. C. Turner, C. Manolatou, B. S. Schmidt, M. Lipson, M. A. Foster, J. E. Sharping, and A. L. Gaeta, "Tailored anomalous group-velocity dispersion in silicon channel waveguides," *Opt. Express* **14**, 4357–4362 (2006).
21. M. A. Foster, A. C. Turner, J. E. Sharping, B. S. Schmidt, M. Lipson, and A. L. Gaeta, "Broad-band optical parametric gain on a silicon photonic chip," *Nature* **441**, 960–963 (2006).
22. J. Kageyama, K. Kintaka, and J. Nishii, "Transmission loss characteristics of silicon nitride waveguides fabricated by liquid source plasma enhanced chemical vapor deposition," *Thin Solid Films* **515**, 3816-3819 (2007).
23. Long Chen, Nicolás Sherwood-Droz, and Michal Lipson, "Compact bandwidth-tunable microring resonators," *Opt. Lett.* **32**, 3361-3363 (2007).
24. B. Miao, P. Yao, J. Murakowski, and D. W. Prather, "Fabrication of silicon microring resonators with narrow coupling gaps," *J. Microlith., Microfab., Microsyst.* **41**, 023013 (2005).

VOLUME II: COST PROPOSAL

1. BAA 08-22: Defense Sciences Research and Technology
2. *Technical Area:* Slow light
3. *Lead Organization:* Cornell University
4. *Type of Business:* Other Educational
5. *Contractor's Reference Number:* N/A
6. *Team Members:* University of Southern California
7. *Proposal Title:* **Large Tunable Delays in Fiber and On-Chip via Conversion/Dispersion**
8. *Technical POC:*
Professor Alexander Gaeta
School of Applied & Engineering Physics
Cornell University
Ithaca, NY 14853
Tel: (607) 255-9983 Fax: (607) 255-7658
e-mail: a.gaeta@cornell.edu
9. *Administrative POC:*
Ms. Diane West
Grant & Contract Officer
Office of Sponsored Programs
373 Pine Tree Rd.
Cornell University
Ithaca, NY 14850
Tel: (607) 255-0655 Fax: (607) 255-5058
e-mail: dw68@cornell.edu
10. *Award Instrument Requested:* Grant
11. *Place of Performance:* Cornell University, University Southern California
Period of Performance: 1.5 years
12. *Total Proposed Cost:* \$2,300,000
13. *DCMA:* Unknown
14. *DCAA:* Raymond Taylor
Office of Inspector General
26 Federal Plaza
New York, NY 10278
15. *Date Prepared:* June 5 2008
16. *DUNS:* 872612445
17. *TIN:* 150532082
18. *Cage Code:* 4B578

CONTENTS

II.B. Detailed Cost Breakdown

II.B.1. By Major Cost Items

II.B.2. Itemization of Equipment Purchases

II.B.3 Projected Funding Requirements by Month

II.C. Supporting Cost and Pricing Information

II.C.1. Cornell University (Gaeta and Lipson)

II.C.2. University of Southern California (Willner)

II.B.1. Detailed Cost Breakdown by Major Cost Items

Cornell University

		PROPOSED BUDGET		
		GAETA		
		Period I	Period II	PROJECT
		7/1/08	5/1/09	TOTAL
		4/30/09	12/31/09	
PERSONNEL:				
Principal Investigator,				
A. Gaeta	Academic Year - 1 Month	\$ 14,418	\$ 2,953	\$ 17,371
A. Gaeta	Summer Salary - 2 Weeks	4,343	4,560	8,903
M. Lipson	Academic Year -2% Effort	3,111	2,613	5,724
M. Lipson	Summer Salary - 1 Month	13,825	14,516	28,341
Research Associates (1)				
Postdoctoral Associates (3.5)				
Graduate Research Assistants (3 in Period I; 2.5 in Period II)				
Total Salaries and Wages				
Fringe Benefits: 7/1/08-6/30/09 33%; 7/1/09 34%				
Total Salaries, Wages & Fringe Benefits				
CAPITAL EQUIPMENT:				
TRAVEL:				
Domestic				
Foreign				
OTHER DIRECT COSTS:				
Materials and Supplies				
Publications/ Communications				
ECE Computer / Lan / Wan				
Cornell Nanofabrication Facility Charges				
SubAward to USC				
Total Other Direct Costs				
TOTAL DIRECT COSTS:				
MTDC Base (Excludes GRA Exclusion & Capital Equip)				
INDIRECT COSTS: 59% MTDC				
TOTAL DIRECT AND INDIRECT COSTS:				

II.B.2. Itemization of Equipment Purchases

Cornell University (Gaeta and Lipson)

Phase III

1. Optical spectrum analyzer	\$15,000
2. Erbium-doped fiber amplifiers, 4 total	44,456
3. Tunable CW laser sources, 3 total	50,544
4. Phase modulator	5,000
5. Electronic spectrum analyzer	15,000
6. Bit error-rate detector	10,000
7. Femtosecond laser	35,000
8. Scanning confocal microscope system	<u>25,000</u>
Total	\$200,000

II.B.3. Projected Funding Requirements by Month

PHASE III:

7/1/08 – 4/30/08 : \$129,000/month

5/1/08 – 12/31/08 : \$126,250/month

II.C. Supporting Cost and Pricing Information

II.C.1. Cornell University (Gaeta and Lipson, and Xu)

Personnel

Salary support is requested for Prof. Gaeta of 1 month of academic-year salary and 2 weeks of summer salary during each year of the project, and 2% Effort is requested for Prof. Lipson. Full-time support is requested for 3.5 postdoctoral associates, 3 graduate students in Period I and 2.5 graduate students in Period II.

Travel

Funds are requested both for domestic and international travel for the PI's, students, and postdocs to conferences, which include LEOS, CLEO, and ECOC meetings.

Materials and Supplies

Funds are requested for standard laboratory equipment which includes, but is not limited to, optical components, electronics, posts, mounts, etc. In addition, funding is requested for fabrication costs at the Cornell Nanofabrication facility for fabrication of Si waveguide structures and devices.

Publications/Communications

Funds are requested to defray costs associated with publishing articles resulting from the funded research. We expect 8 articles and in addition, costs for office supplies, postage and shipping, toll calls, and duplication are also included.

Indirect Costs

Indirect costs are calculated on a MTDC basis at the Institution's federally approved rate of 59%, excluding tuition, capital equipment, and subcontracts. In addition, a 59% off-campus rate is applied to \$25,000 of the subcontract.

II.C.1. University of Southern California (Willner)

COST ESTIMATE - Subaward from Cornell University			Phase III
DARPA DSO: "Large Tunable Delays in Fiber and On-Chip via Conversion/Dispersion"			18 months
Principal Investigator - ALAN E. WILLNER, U	1-Jul-08	1-May-09	1-Jul-08
Period: 1 July 2008 to 31 December 2009	30-Apr-09	31-Dec-09	31-Dec-09
SALARIES and WAGES			
Principal Investigator			
<i>Prof. Alan Willner</i>			
20% effort 15.5 academic	31,780	19,367	51,147
100% 1.5 summer month		28,041	28,041
<i>Post-Doctoral Associate</i>			
50% effort 18 months	18,750	15,450	34,200
Base Salary 08-09, \$45,000/12 mos.			
Total Salary subject to FB	50,530	62,858	113,388
FRINGE BENEFITS			
FY 08 FB & Beyond	27.50%	13,896	17,286
(Total Fringe Benefit)	13,896	17,286	31,182
Research Assistant III			
2 Graduate Students			
50% Effort 15.5 Academic Months	35,511	21,641	57,152
100% Effort 4.5 Summer Months	12,384	25,067	37,451
Base Salary 07-08 \$37,152/9 mos.			
Base Salary 08-09 \$37,600/9 mos.			
Total Salary not subject to FB	47,895	46,708	94,603
TOTAL COMPENSATION	112,321	126,851	239,172
EQUIPMENT	200,000	75,000	275,000
MATERIALS AND SUPPLIES			
Lab components, software licenses, computer upgrades	60,000	59,621	119,621
TRAVEL	4,930	4,930	9,860
Breakdown below			
TUITION			
6 units per RA @ 1,263/unit (07-08) (for 50% GRAs)	13,208	10,888	24,096
TOTAL DIRECT COSTS	390,459	277,290	667,749

F & A Base (Total Direct Costs less equipment and tuition)			
<i>FY 08 F & A Base</i>		177,251	177,251
<i>FY 09 F & A Base</i>			191,402
<i>FY 10 F & A Base</i>			191,402
<i>FY 11 F & A Base</i>			
		177,251	191,402
			368,653
INDIRECT COSTS (F & A)			
<i>FY 08 F & A</i>	63.00%	111,668	111,668
<i>FY 09 F & A</i>	63.00%		120,584
<i>FY 10 F & A</i>	62.00%		120,584
<i>FY 11 F & A</i>	62.00%		
Total Indirect Costs		111,668	120,584
			232,251
TOTAL PROJECT COSTS		502,126	397,874
			900,000

(USC) Notes:

An annual 4% increase in salaries has been calculated for the PI beginning 8/16/08.

An annual 4% increase in salaries has been calculated for the Research Assistants beginning 8/16/09.

An annual 4% increase in salaries has been calculated for the Research Associate beginning 07/01/2009

An annual 4% increase in Tuition has been calculated beginning 8/16/09.

The University has changed the start of the academic year from 9/1 to 8/16 beginning 8/16/2004.

The University has changed the start of the academic year from 9/1 to 8/16 beginning 8/16/2004.

Federal FB language

The fringe benefit rate for the period July 1, 2007 is 27.5.

as approved in the Federal Rate Agreement dated March 21, 2007.

Federal IDC language

For the period beginning 7/1/2004 and ending 6/30/2005, 34.0%

For the period beginning 7/1/2005 and ending 6/30/2006, 32.0%

The following are estimated rates for future periods:

For the period beginning 7/1/2006 and future periods, 32.0%

30.0% should be used as a forecasted rate for future periods.

The predetermined indirect cost rate in the Federal Rate Agreement dated March 21, 2007:

For the period beginning 7/1/2008 and ending 6/30/10, 63%

For the period beginning 7/1/2006 and ending 6/30/08, 63.0%

62.0% should be used starting 7/01/2010 and as a forecasted rate for future periods.

Information not be distributed outside of the Agency.

There may be minor differences in the above calculations due to rounding.

Hourly Rates

In accordance with OMB Circular A-21, the University certifies and collects labor costs by Level of Effort and not hours. Hours are provided for information only as requested by the Sponsor and the Customer.

TRAVEL BREAKDOWN

East Coast Trips each (Airfare=\$550, Registration=\$500,
Hotel and Meals \$170x3=510, Total per trip \$1,560.)

TRAVEL	1st period	2nd period
East Coast	2	2
West Coast	2	2

West Coast Trips each (Airfare=\$125, Registration=\$500,
Hotel & Meals=\$140x2=\$280, Total per trip= \$905)

Conferences include: IEEE Conferences and Workshops; OFC meetings and conferences.



June 4, 2008

Cornell University, Office of Sponsored Programs
ATTN: Diane L. West, Grant & Contract Officer
373 Pine Tree Road
Ithaca, NY 14850-2820

Department of
Contracts and Grants

SUBJECT: Proposal in Response to DARPA DSO
Entitled: *"Large Tunable Delays in Fiber and On-Chip via
Conversion/Dispersion"*

Principal Investigator: Alan E. Willner, Ph.D.
Period of Performance: July 1, 2008 – December 31, 2009
Total Amount Requested: \$900,000.00

We are pleased to forward the subject proposal for your consideration and approval. This proposal has been approved by the administration of the University. If awarded, we request a cost-reimbursement subaward and anticipate negotiating mutually agreeable terms.

Should you have any questions of a technical nature regarding this proposal, please contact the Principal Investigator. Information of a business or administrative nature should be directed to the attention of Jeffrey Sparks, Contract and Grant Administrator, by phone (213)740-6119, fax (213) 740-6070, or by e-mail JSparks@ooc.usc.edu.

Sincerely,

A handwritten signature in cursive script, appearing to read "Barbara N. Lewis", is positioned above the typed name.

Barbara Lewis
Deputy Director

cc: Principal Investigator
File

University of
Southern California
Los Angeles,
California 90089-1147
Tel: 213 740 7762
Fax: 213 740 6070
Web page:
[www.usc.edu/dept/
contracts/](http://www.usc.edu/dept/contracts/)